Response to Reviewers:

(1) Response to Referee Comment 1 (RC1)

"This study investigates the temperature effect on the formation of highly oxidized molecules (HOMs) from the a/b-pinene ozonolysis. The authors found that temperature plays a controlling role in the yields of HOMs: the molar yields dropped by around a factor of 50 when experiments were performed at 273 K, compared to 293 K. Interestingly, the distribution of HOMs molecules is not significantly affected by the temperature, that is, the formation rates of more oxidized HOMs did not decrease more than the less oxidized HOMs. A possible explanation, as the authors proposed, is that the rate limiting step forming these HOMs occurs before the products become oxygenated enough to be detected by the CIMS instrument used in this study. Overall the paper is well written and approaches an important aspect of atmospheric nucleation processes. Yet there seem to be various uncertainties in the quantitative representation of HOMs formation and comparison under different temperature scenarios, see detailed comments below."

We thank the reviewer for the positive feedback and will answer the comments point-by-point below:

Comment 1: **"Temperature plays a governing role in the SOA formation by affecting the vapor pressure of the condensing molecules. The vapor pressure of any given molecule may decrease by orders of magnitude as the temperature drops to certain degrees. As a result, the SOA yield from the oxidation of a given hydrocarbon like a-pinene at low temperature (e.g., -15 C) is expected to be significantly higher than at room temperature. This in turn provides more surface area to absorb more organic vapors from the gas phase to the particle phase. It is therefore not surprising that the observed gas-phase concentrations of HOMs are lower at low temperature. However, the authors did not take into account of this effect when drawing the conclusion that 'the HOMs molar yields dropped by around a factor of 50 when experiments were performed at 273 K compared to 293 K'. The vapor pressure and saturation concentration of each HOM molecule can be estimated based on the carbon and oxygen numbers (see 2D VBS paper as an example) in the molecule. With the measured total aerosol mass concentration, the authors should be able to estimate the fraction of each HOM molecule in the particle phase vs. gas phase at equilibrium at different temperatures. Or the authors can compare the calculated condensational sinks at different temperatures and evaluate the impact of changes in condensational sinks on the estimated molar yields of HOMs."**

Reply to Comment 1: The reviewer is correct that a decrease in temperature will decrease the vapor pressure of molecules, thereby forming more SOA. However, in our study, we accounted for this effect by explicitly including the condensation sink (CS) in our HOM yield estimation (see Eq. 2 and section 2.5.). Thus, the reported decrease of a factor ~50 in HOM yield between 20 and 0 degrees already accounts for the difference in CS between the two temperatures.

The condensation sink was calculated for each experiment based on aerosol size distribution measurements with a Scanning mobility particle sizer (SMPS). As an example, in the experiments with [α-pinene] = 50 ppb, 40 min after α-pinene injection, the calculated CS was 6.2 10^{-2} s^{-1} at 20 °C (12-Jan-2017), and 8.1 10^{-2} s^{-1} at 0 °C (16-Jan-2017). In other words, the CS increased ~30 %, while the HOM signals decreased by more than 98%, clearly indicating that the CS is not the main driver for the decreased HOM concentrations. A comparison of the evolution of condensation sinks for a few experiments performed at different conditions is shown below in Figure R1.1.

<u>Comment 2:</u> "The authors used a simplified expression for the HOMs molar yield (Eq 2). The authors assume that all HOMs molecules are first-generation oxidation products and the only source of HOMs is the apiene+O3 reaction. While this assumption seems reasonable for the monomers, it does not seem to work adequately for the dimers, as shown in Figure 5. In the expression of the condensational sinks, the authors stated that the loss rate on the wall is ~10-3 s-1. Many studies have shown that the loss rate of individual molecules depends on their molecular weight or vapor pressure. Is the value of ~10-3 s-1 representative of the loss rate of monomers or dimers? In the presence of relatively little number of particles at the beginning of low aerosol loading experiments, is the wall loss rate still much lower than the particle condensation rate? Same for the representation of condensation on particles, a single value for the case of C10H16O7 is applied to all HOMs molecules. Have the authors estimated the uncertainties associated with this simplified treatment?"

<u>Reply to Comment 2:</u> We estimate our wall loss rate to be on the order of 10^{-3} s^{-1} based on earlier studies, e.g. Ehn et al. (2014) who measured a value of ~10^{-2} s^{-1} for the wall loss rate of HOM in a 1.5 m^3 chamber with active mixing assisted by a fan. The AURA chamber is ~3 times larger than the chamber used in that study, and without mixing, and therefore the wall sinks for HOM much lower, likely even below 10^{-3} s^{-1}. This value can be compared to the typical CS values during the experiments, e.g. as shown in Figure R1.1, which are much larger. As also described in section 2.5, based on earlier work, HOM are expected to condense irreversibly onto walls and particles, whether monomers or dimers. Thus, the exact vapor pressures will not influence the loss rates of different HOM. However, the larger dimers will move more slowly, causing their loss rates to be slightly lower than the smaller monomers. The variety of HOM-products formed upon monoterpene ozonolysis includes compounds from 308 Th to 622 Th, with compounds containing 10 to 20 carbon atoms and 7 to 19 oxygens. Figure R1.2 shows an estimation of the net condensation sink for a few example molecules at 20 °C, with [α-pinene] = 50 ppb (12-Jan-2017). The difference between the smallest monomer and one of the largest dimers is on the order of 30%, which is close to the uncertainty of the CS calculation itself, as the exact structures of the HOM are not known. Hence, we concluded to use the representative value of one of the most abundant HOM for the analysis. We added a sentence to section 2.5 about the uncertainty of a few tens of percent that arises from this simplification. But we again emphasize that this uncertainty is marginal compared to the factor of 50 increase in HOM yield between the 20- and 0-degree experiments.

In Figure 5, which the reviewer refers to, we show the resolved molar yield based on Eq. 2 for each HOM molecule. At 20 °C and 0 °C, the method used showed good results and reliability (goodness of fit indicated by the color coding and sizing of the markers), while at -15 °C, the fits were poor due to the very low HOM signals. We interpret the reviewer's comment about our assumptions "not working adequately for the dimers" to concern the inset figure, where the fit for the dimer shows much more scatter. However, these inset plots merely show examples with $C_{10}H_{14}O_9$ and $C_{19}H_{28}O_{12}$ to better visualize a 'good fit' (r^2 = 0.99) and a 'bad fit' (r^2 = 0.62) at 20 °C. The quality of the fit is

due to the much lower concentration of the dimer in this example, and is not a result of the molecule being a dimer to begin with. This can also be clearly seen from the color coding in Figure 5, where dark blue markers ($r^2 > 0.9$) are abundant also in the dimer range. This result is also in line with the current knowledge of the formation mechanism of these dimers from peroxy-radical cross reactions (e.g. Bianchi et al., 2019), i.e. also the dimers are first-generation oxidation products.

Finally, all our experiments were performed with practically zero initial particles at the beginning of the experiment. Therefore, it is clear that in the first minutes of each experiment, the assumption that CS dominates over the wall loss will not hold. However, at this stage the chamber is still not homogeneously mixed either, and we did not include data from the first 40 minutes in our calculations for the HOM yield. We note that this was not clearly stated in the manuscript and we have now added this information to section 3.4. in the text and in the legend of Figure 5. After these 40 minutes, the CS was always clearly higher than the wall loss rate. E.g., in the case of low VOC loadings (02-Dec-2016), the calculated CS was $1.2\ 10^{-2}\ s^{-1}$ after 40 min.

Comment 3: **"It is well-known that HOMs are easily deposited on the chamber wall or the CIMS inlet. However, factors that likely impact the HOMs loss rate are still unclear. Have the authors performed any characterization experiments on the temperature effect on the wall loss rate? For experiments conducted at low temperature, e.g., -15 C, was the chamber air drawn directly to the CIMS inlet? Would the mixing of the chamber air with room temperature sheath air cause any turbulence inside of the inlet? Would any turbulence cause any unstable signals or intensive loss of HOMs?"**

Reply to Comment 3: The optimal sampling with the CI-APi-TOF is indeed a challenge when the sample air temperature is different than room temperature, whether the sample is cold ambient air or from a cooled chamber, as in this study. We performed the measurements in a similar way for all temperatures in the chamber, as our larger concern was that sampling colder (i.e. denser) air into the mass spectrometer could alter the pressures, and therefore the performance, of the instrument. In order to assure the validity of our results, we carefully examined the pressures and reagent ion count (RIC) data as described in section 3.1 "Effect of the temperature on the CI-APi-TOF". For the two highest temperatures, the RIC remained the same, but at -15 °C the RIC is slightly lower by roughly 15%. This change is likely due purely to instrumental effects caused by sampling the colder air. However, this change was again minor when comparing to the dramatic changes seen in the HOM concentrations, indicating that changes inside the instrument were unlikely to be the cause for our results.

Concerning turbulence/mixing inside the CI inlet, it is possible that air of different temperatures could cause some additional mixing, but as the reagent ions are pushed electrostatically into the sample air in the beginning of the drift tube, added mixing (leading to losses of HOM) would also cause a similar loss of the reagent ions. This was not observed, and would still, to a certain extent, have been corrected for by the normalization of HOM signals to the RIC. Thus, our observations indicate that instrumental effects could only explain a small fraction of the changes we observed in the HOM yields. We added some more details of the sampling protocol to the manuscript in section 2.4.

Comment 4: **"It seems like experiments conducted at ~30 C are likely more representative of the intensive photochemistry of biogenic emissions at summertime, compared with the conditions in the current study, i.e., -15 C, 0 C, and 20 C."**

Reply to Comment 4: It would certainly be of interest in future work to map out a wider temperature range, with many more points than we were able to in this study. The probed range in this work does cover a large fraction of the expected temperatures in e.g. the boreal forest. We also note that we did not focus on photochemistry, but rather the ozonolysis of monoterpenes, which takes place also during nights.

Additional Figures (For referee comment reply only):

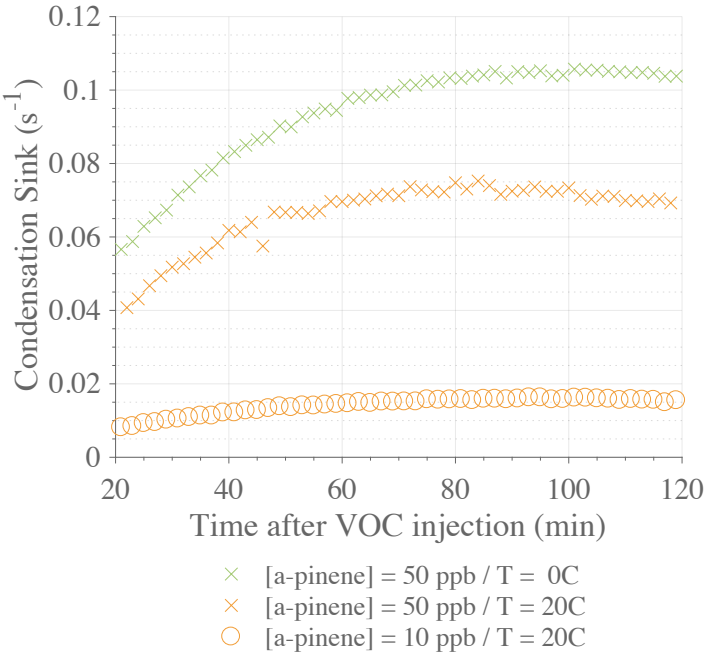

Figure R1.1: Comparison of the Calculated condensation sinks over the ACCHA runs. Data shown from 20 min to 120 min after α-pinene injection for experiments performed at 50 ppb at 0 °C (16-Jan-2017) - green crosses, and 20 °C (12-Jan-2017) – red crosses, and at 10 ppb at 20 °C (12-Dec-2016) – red circles.

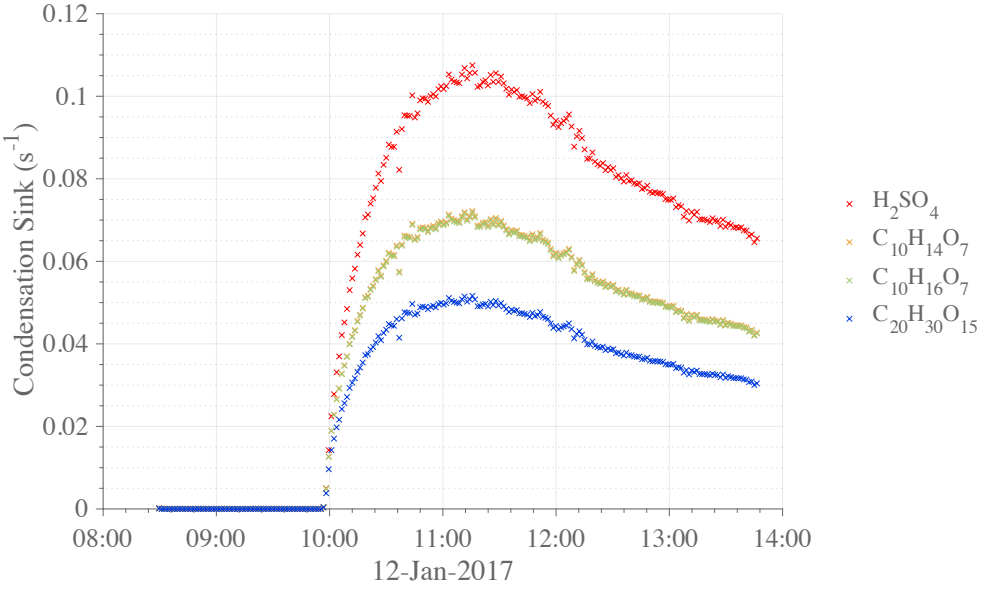

Figure R1.2: Comparison of estimated condensation sinks for Sulfuric acid (red crosses), $C_{10}H_{14}O_7$ (orange crosses), $C_{10}H_{16}O_7$ (green crosses), and $C_{20}H_{30}O_{15}$ (blue crosses) during a high loading experiment (i.e. [α-pinene] = 50 ppb) at 20 °C (12-Jan-2017).

References:

Bianchi, F., Kurtén, T., Riva, M., Mohr, C., Rissanen, M. P., Roldin, P., Berndt, T., Crounse, J. D., Wennberg, P. O., and Mentel, T. F.: Highly Oxygenated Organic Molecules (HOM) from Gas-Phase Autoxidation Involving Peroxy Radicals: A Key Contributor to Atmospheric Aerosol, Chemical Reviews, 2019.

Ehn, M., Thornton, J. A., Kleist, E., Sipilä, M., Junninen, H., Pullinen, I., Springer, M., Rubach, F., Tillmann, R., and Lee, B.: A large source of low-volatility secondary organic aerosol, Nature, 506, 476, 2014.

(2) Response to Referee Comment 2 (RC2)

"The authors studied the formation of HOM (highly oxygenated organic molecules) by ozonolysis of a-pinene (and b-Pinene) and determined molecular HOM yields as a function of the temperature. Experiments were performed in the AURA chamber. HOM were measured by NO3-CIMS. The findings are an interesting and important puzzle piece in finding out about the importance of HOM for SOA formation and atmospheric chemistry in general, as the temperature range was extended to -15°. Background for the study is that HOM formation should be hampered at low T, as the key formation step the rearrangement of peroxy radicals should be strongly dependent on temperature. The thorough study was a challenge and has some "weak points", the main being the quantification of the HOM: even comparison of relative HOM pattern maybe difficult at different temperatures. As consequence the findings have some uncertainties. However, the authors addressed these issues and dealt with them quite clear and openly. Thus manuscript provides a new and original contribution for understanding HOM. The manuscript is highly interesting and very well written. I have only minor comments dealing with the quantification and some small remarks. I suggest to publish this very interesting manuscript in ACP. It could be even publish as it is, but the authors may want to consider the comments below."

We thank the reviewer for the positive feedback and will answer the comments point-by-point below:

Comment 1: "line 185: ". . .the calibration factor C = 1.65E9 molecules cm-3", the reference to it is pretty vague. Do I understand correctly that you detect about 70 ppt HOM per normalized ct? Can you add your detection limit? "

Reply to comment 1: The reviewer is correct that we detect ~70 ppt HOM per normalized count, and we added this also to the manuscript for clarity. Reporting a calibration factor of the type used here has become customary for the CI-APi-TOF, although most other similar instruments report sensitivities as cps/ppt. We also added our detection limit estimate.

Comment 2: "line 269: Did you try to verify your transmission function? Ehn et al. 2011 and Heinritzi et al. 2016 show quite different transmission behavior."

Reply to comment 2: Unfortunately, we did not have the chance to do such a measurement. The transmission can indeed vary considerably based on the specific tuning of the instrument. In our study the calibration factor C was lower than typically reported, which may be an indication of relatively low transmission at the reagent ion masses. As we mainly look at the relative changes of HOM, the transmission function is ultimately of less concern in our study.

We also note that the transmission curves of Heinritzi (Fig 5a) and Ehn (Fig. 2d) look different mainly due to the selected curve type by which they are represented. The data points in these two plots are

in fact fairly consistent, with the exception of the overall higher transmission in the instrument used by Heinritzi et al.

Comment 3: **"line 270: How did you specifically estimate the uncertainty of tens of percent? From the variation of the RI 5-7E4 cps? (I guess you meant "several times 10%"?)"**

"We conclude from the above investigations that changes on the order of tens of percent occurred in our instrument as the AURA chamber temperature was varied, and that only signal changes larger than this should be attributed to actual perturbations in the chemistry taking place in the chamber.**"**

Reply to comment 3:

This is correct, it was based on the RIC variation, and we have now added this more clearly into the main text.

Remarks:

(1) "line 142: "In practice, the experimental plan focused on α-pinene oxidation. . .", sounds a little skewed. Maybe better "The experiments focused on α-pinene oxidation..."

(2) "line 373 and line 378: I suggest to reformulate this sentence. Despite your large uncertainty you still "calculate" the yields. They maybe only estimates because of the uncertainty. . .. Accordingly you should replace "absolute estimates" by "molar yields" in line 378. "

(3) "Figure 3, legend: I suggest to replace "HOM spectrum" by "selected HOM". It is easier to grip."

Reply to remarks: Thanks for the suggestions, the text was modified accordingly.

References:

Ehn, M., Thornton, J. A., Kleist, E., Sipilä, M., Junninen, H., Pullinen, I., Springer, M., Rubach, F., Tillmann, R., and Lee, B.: A large source of low-volatility secondary organic aerosol, Nature, 506, 476, 2014.

Heinritzi, M., Hansel, A., Simon, M., Steiner, G., Wagner, A. C., Kürten, A., and Curtius, J.: Characterization of the mass-dependent transmission efficiency of a CIMS, Atmos. Meas. Tech., 9, 1449-1460, 2016.

(3) Reply to the Review (RC3)

"This study investigated the effect of temperature on HOMs formation from α-pinene oxidation. Experiments were conducted at three different temperatures (20, 0, and -15°C). It is found that HOMs formation considerably decreases as temperature decreases. It is also claimed that the distributions of HOMs at 20°C and 0°C are very similar, which is conjectured to be due to that the rate-limiting step forming these HOMs occurs before the products become oxygenated enough to be detected by NO3- CIMS. This work investigated the effect of temperature on HOMs formation, which is important to help us further understand the formation mechanism of HOMs. However, there are a number of issues that need to be addressed before the paper can be published."

We thank the reviewer for the positive feedback and will answer the comments point-by-point below:

Comment 1: "The major issue involves the comparison of HOMs distribution between 20°C and 0°C. While the authors claim that the distributions are very similar between two temperatures, I beg to differ. Let's start by looking at Figure 3. By eyeballing, the dominant monomer signal at 20°C ~308 amu, but it was ~325 amu at 0°C. There is also clear difference in the range 350-360 amu between two temperatures.

Reply to comment 1: In Figure 3, we showed example spectra taken 10 min after α-pinene injection in all the temperature studied, since this was the period when the HOM typically were at their highest. Some precaution should be taken when analyzing those spectra as the chamber might not have been well-mixed yet at this time. This is also the reason for why our main analyses only include periods starting 40 min into the experiments (see also response to reviewer 2). Despite this, we do not find our original conclusion of a rather similar distribution too erroneous; we aimed at emphasizing that all identified compounds considered as HOM are present in the spectra at all the temperatures, and more importantly that there is no clear change in the spectral distribution as a function of oxygen content.

However, after considering the present comment, at the choice to use data 10 min after injection of the VOC may be misleading for a spectral comparison. In Figure R3.1, we instead plot the spectra averaged between 40 min and 120 min after α-pinene injection. This time period is the one used for figures 5 and 6, and this figure will now replace the original Figure 3 The HOM distribution is also shown in the form of a pie chart, as suggested by the reviewer in a later comment, in Figure R3.2, where we represented the HOM fraction – larger than 1% - for high loading experiment at 20 °C, 0 °C and -15 °C. From these plots the comparison is not trivial as only the largest HOM contributors are easy to distinguish, and the smaller signals, e.g. dimer species cannot be compared. Hence, we continued our analysis by plotting the HOM signal intensities measured at 0 °C vs those measured at 20 °C in Figure R3.3. From these figures it becomes clearer that the majority of the HOM signal intensities decreased close to a factor 50 (as depicted by the 1:50 solid line, and with most molecules within the bounds of the 1:25 and 1:100 dashed lines). The most abundant monomer signals are some of the few HOM that show clearly larger discrepancies, but overall, we retain that the spectra can be described as fairly similar. Also, importantly, we cannot isolate any trend related to the oxygen content, which supports our main conclusion: the temperature mostly influences the initial steps of the autoxidation rather than the successive oxygen additions during the HOM formation. Figure R3.3b was now added to the manuscript as a new Figure 7 in section 3.4.

Comment 2: **"As there are various HOMs formation pathways, it is likely that temperature has different effects on distinct pathways. This brings up one critical issue in the data interpretation - as there are both α-pinene + OH and α-pinene+O3 and the isomerization rates of RO2 from different oxidants are different, I suggest the authors to discuss the temperature effect on two channels separately."**

Reply to comment 2: The reviewer is correct that the isomerization rates of RO2 are different, but not only for the products from the different oxidation pathways, but indeed for every single RO2. For example, in the ozone reaction, four different RO2 structures are formed, each having different isomerization rates (Kurtén et al., 2015, JPCA). With the data available to us in this study, we are not able to speculate about how the temperature would affect different RO2 separately. We focus our discussion on the ozone pathway for a few reasons: as mentioned in the methods section 2.2, model simulations estimate oxidation processes to be about 2/3 for ozonolysis and about 1/3 for the OH reaction. Additionally, Jokinen et al. (2015) showed that the HOM yield from OH oxidation is ~10x lower than that of ozonolysis. Therefore, we expect ozonolysis to be the dominant pathway.

Comment 3: **"To continue, the conclusion is drawn mainly based on Figure 6, and the authors noted that there is no clear trend in the yield change for any column. Again, I beg to differ. Take C10H16 column as an example. There is a weak increase in yield ratio (light green → ♉blue) with more oxygen. For C18H28 column, there seems to be a decrease in yield ratio.**

Reply to comment 3: For evaluating the goodness of fit for determining the HOM yields at different temperatures, we implemented a r^2*r^2 information by the size of the squares. In the examples mentioned by the reviewer, $C_{10}H_{16}O_x$ and $C_{18}H_{28}O_y$, ratios involve r^2*r^2 that are below 0.25 which implies a lack of reliable data for isolating a clear trend in our dataset. In addition, even in these columns, the trends pointed out by the reviewer only concern a few of the molecules. In neither case is there a trend line that would contain more than half of the data points in a column, and statistical variability alone will certainly cause apparent trends over a few data points.

Comment 4: "One figure **I suggest to make is a pie chart to show the fraction of each HOM in total HOMs**. By comparing the pie charts between two temperatures, it would be easier to examine the temperature effect on HOMs distribution."

Reply to comment 4: See reply to comment 1 & Figure R3.2

Comment 5: **"Still in Figure 6, why are only five HOM monomers included? There are clearly more HOMs as shown in Figure 3 and Table A2. As a side note, because autoxidation would add two oxygen atoms, it is not proper to present the HOMs formation by +1 oxygen as shown in Figure 6.**

Reply to comment 5: In Figure 6, there are 10 HOM-monomers plotted, and these are all the identified closed shell species. Compounds with an odd number of H-atoms are radical species, and

their yields cannot be calculated without knowing their reaction rate constants with all other RO2. In the yield calculation for the closed shell HOM species, the CS is the major sink term, but for the radicals this is not the case, and therefore they are not plotted in neither Fig. 5 or 6.

The figure itself does not show any formation mechanisms, only the variety of measured HOM compounds with their specific yield ratio. Therefore, we do not find it improper to present the data this way.

Comment 6: "Lastly, one thing to consider when discussing the temperature effect is the RO2 fate. As the temperature decreases, the RO2+RO2 and RO2+HO2 react rates will also decrease, which increase bimolecular lifetime and enhance the fraction that undergoes isomerization. It would be helpful to quantify the RO2 bimolecular lifetime (Line 435)."

Reply to comment 6: Once the peroxy-radical species is formed, 3 terminations type could occur: (1) bimolecular reaction on the type of RO_2 + RO_2, (2) termination by HO_2 or (3) unimolecular reaction. As shown in Berndt et al. (2018), the reaction rate between RO_2 + RO_2 highly depend on the composition of the species involved in the recombination: every single RO_2 will react at a different rate with another $R^{'}O_2$ (or with HO_2, alternatively) This results in a wide range of reaction rates that can vary by several orders of magnitude. However, bimolecular reactions generally have low energy barriers and thus would not be strongly dependent on temperature, at least if compared to the unimolecular reactions. If this wouldn't be the case, our measurement should show a big variation in the ratio monomers-to-dimers, which is not the case. While we do agree that it would be interesting to assess the bimolecular lifetimes, our data set does allow such an analysis.

Remarks:

1. How is time-dependent d[HOM]/dt calculated?

We obtained d[HOM]/dt simply from our measured HOM signal, as the change Δ[HOM] between two data points Δt.

2. It would be useful to show the equation to calculate the CS, even included in supplement.

The CS was calculated according to Dal Maso et al., 2005 with refined parameters as mentioned in the method section 2.5. We added the missing reference in the manuscript.

3. Can the authors please describe the sampling lines and inlet? Some discussion of the losses in sampling line and inlet is warranted.

We added a description of the inlet and the CIMS sampling line in the manuscript in section 2.4: "The instrument sampled air at about 80 cm from the wall of the chamber via a ¾ inch tube directly connected to the CI-APi-TOF, which was located outside the chamber enclosure (~20 °C at all time). The sheath air (taken from a compressed air line) was 30 LPM and the total flow (generated by the house vacuum line) was 40 LPM. The ~1 m long inlet had a flow of 10 LPM caused by the difference

between the sheath and total flows. With such a tube length and flow, roughly half of the HOM are expected to be lost to the walls of the inlet lines."

4. It would be useful to show the [SOA] under different temperature. Or a plot to compare the CS between different temperatures.

A much more detailed particle analysis from this campaign will be presented in a separate paper (Kristensen et al., in prep), and therefore we have not included specifics on the aerosol data here. We show below, in Figure R3.4, a comparison of the condensation sinks at different temperature for reference.

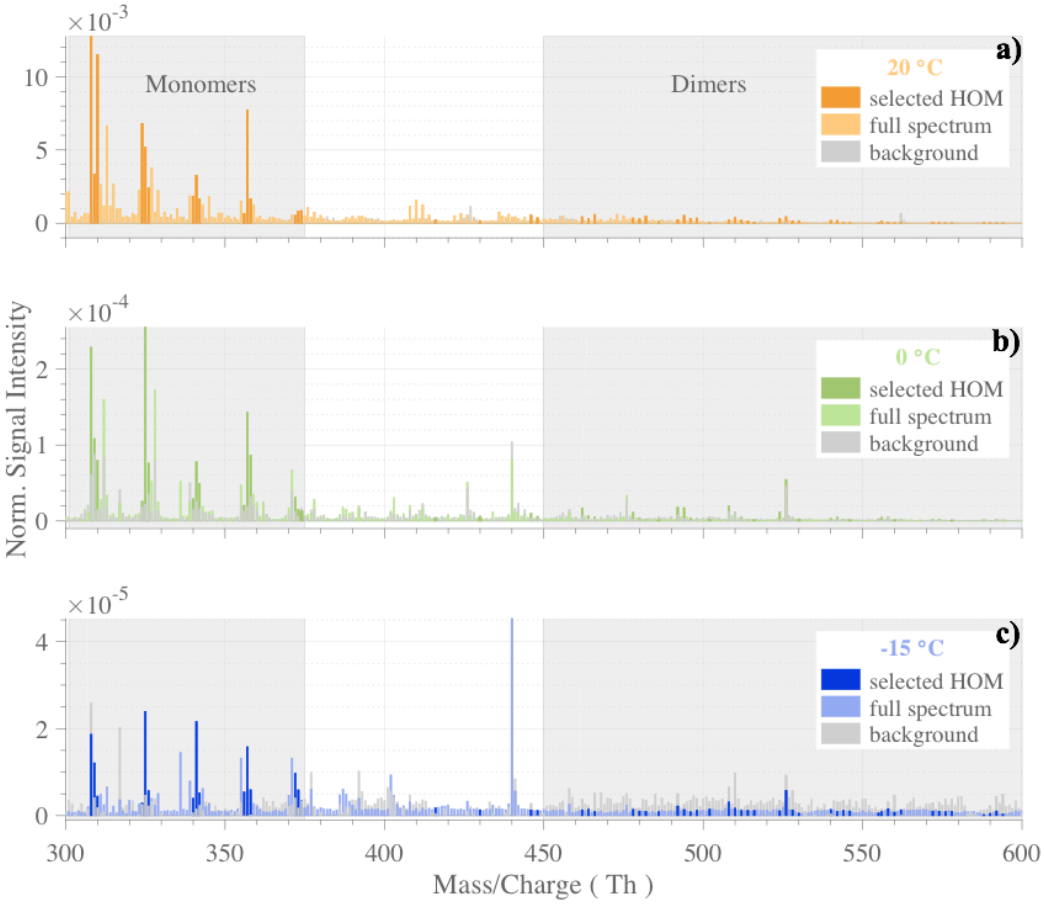

Figure R3.1 (also new Figure 3 in MS): Typical HOM mass spectra observed during α-pinene ozonolysis experiments (initial conditions: [α-pinene] = 50 ppb, [O3] = 100 ppb,) at T = 20 °C (panel a) in orange, T = 0 °C (panel b) in green, T = -15 °C (panel c) in blue. The normalized signals were averaged over 5 minutes during background measurement before VOC injection (gray bars), and from 40 min to 120 min after α-pinene injection (colored bars). Specific masses, selected for representing high-intensity HOM, are highlighted in darker colors. Gray-shaded areas show HOM sub-ranges of monomers and dimers.

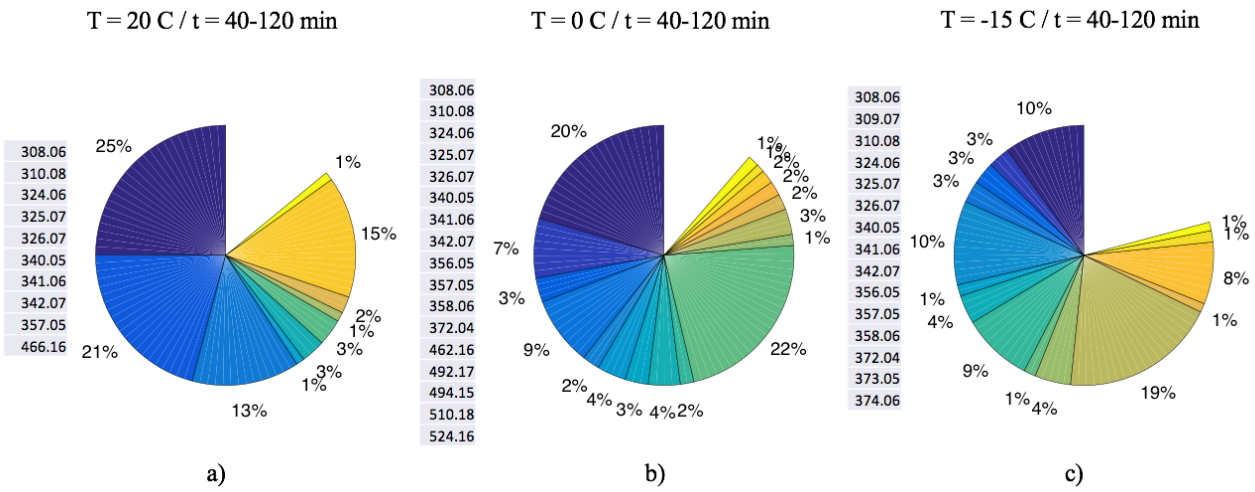

Figure R2.2: Evaluation of HOM fraction from 40 min to 120 min after α-pinene injection at 20 °C (panel a), 0°C (panel b) and -15 °C (panel c). Masse to charge ratios (in Th) are indicated on the left side of each panel where the first compound represents the darkest blue fraction. The 'missing' portion is the sum HOM contributions that are lower than 1 %.

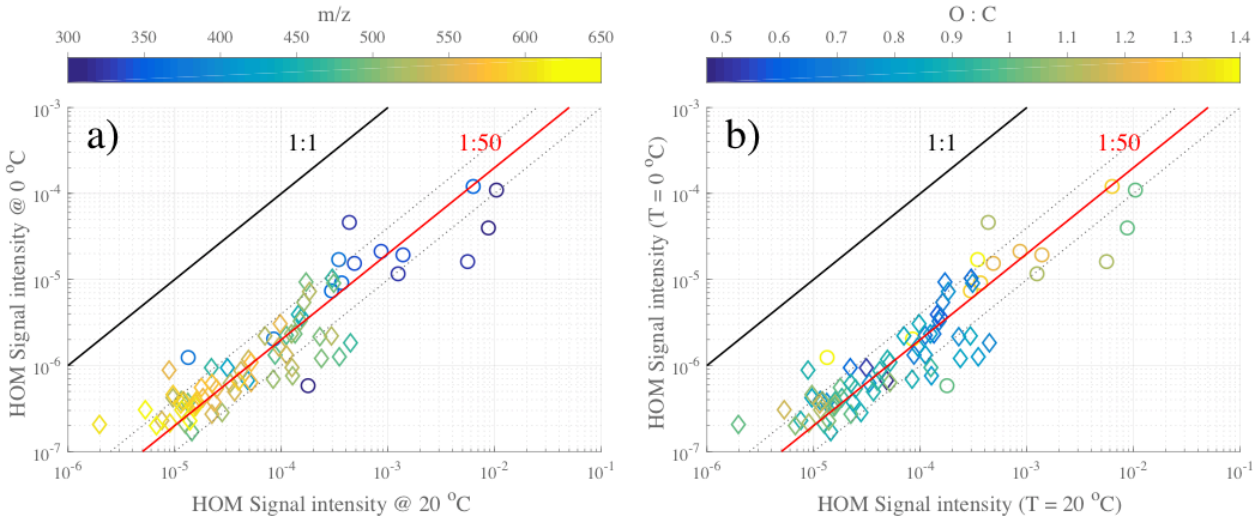

Figure R3.3: Scatter plot on the HOM normalized signal intensity at 0°C and at 20 °C. The data points are colored by the mass-to-charge ratio (panel a) or by oxygen-to-carbon ratio (panel b) with distinction between monomer – circle markers - and dimer compounds – diamond markers. Guide lines were added as indicators: 1:1 line – in black, 1:50 line – in red ,1:25 and 1:100 lines - in dotted grey. **Figure R3b) was added to the manuscript as Figure 7.**

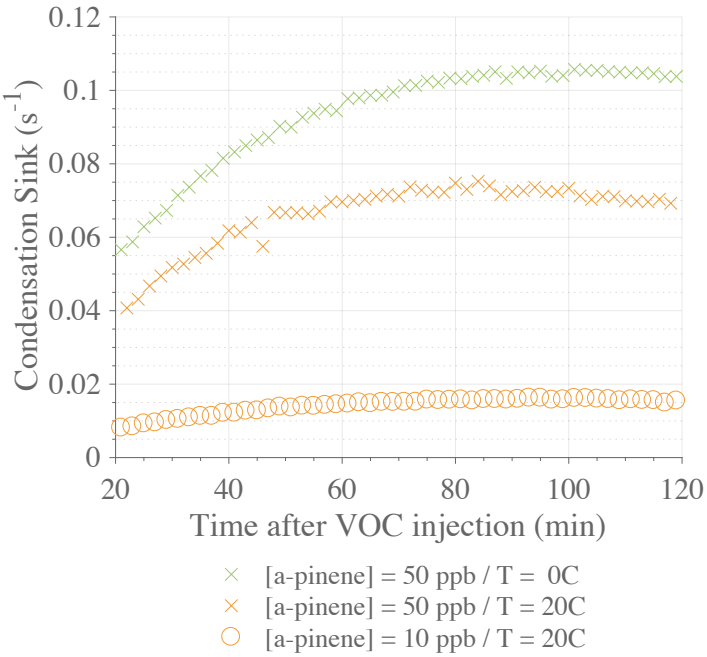

Figure R3.4: Calculated condensation sinks over some ACCHA runs. Data shown from 20 min to 120 min after α-pinene injection for experiments performed at 50 ppb at 0 °C (16-Jan-2017) - green crosses, and 20 °C (12-Jan-2017) – red crosses, and at 10 ppb at 20 °C (12-Dec-2016) – red circles.

References:

Berndt, T., Scholz, W., Mentler, B., Fischer, L., Herrmann, H., Kulmala, M., and Hansel, A.: Accretion Product Formation from Self-and Cross-Reactions of RO2 Radicals in the Atmosphere, Angewandte Chemie International Edition, 57, 3820-3824, 2018.

Dal Maso, M., Kulmala, M., Riipinen, I., Wagner, R., Hussein, T., Aalto, P. P., and Lehtinen, K. E.: Formation and growth of fresh atmospheric aerosols: eight years of aerosol size distribution data from SMEAR II, Hyytiala, Finland, Boreal Environment Research, 10, 323, 2005.

Jokinen, T., Berndt, T., Makkonen, R., Kerminen, V.-M., Junninen, H., Paasonen, P., Stratmann, F., Herrmann, H., Guenther, A. B., and Worsnop, D. R.: Production of extremely low volatile organic compounds from biogenic emissions: Measured yields and atmospheric implications, Proceedings of the National Academy of Sciences, 201423977, 2015.

Kristensen, K., Normann-Jensen, L., Quéléver, L. L. J., Rosati, B., Elm, J., Teiwes, R., Pedersen, H. B., Glasius, M., Ehn, M. and Bilde, M.: The Aarhus Chamber Campaign on Highly oxidized multifunctional organic molecules and Aerosols (ACCHA): Particle formation and detailed chemical composition, *Manuscript in preparation*.

Kurtén, T., Rissanen, M. P., Mackeprang, K., Thornton, J. A., Hyttinen, N., Jørgensen, S., Ehn, M., and Kjaergaard, H. G.: Computational study of hydrogen shifts and ring-opening mechanisms in α-pinene ozonolysis products, The Journal of Physical Chemistry A, 119, 11366-11375, 2015.

Manuscript (Changes marked in orange):

Effect of temperature on the formation of highly oxygenated organic molecules (HOM) from alpha-pinene ozonolysis

Lauriane L. J. QUÉLÉVER [1], Kasper KRISTENSEN [2*], Louise NORMANN JENSEN [2], Bernadette ROSATI [2,3], Ricky TEIWES [2,3], Kaspar R. DAELLENBACH [1], Otso PERÄKYLÄ [1], Pontus ROLDIN [4], Rossana BOSSI [5], Henrik B. PEDERSEN [3], Marianne GLASIUS [2], Merete BILDE [2] and Mikael EHN [1].

[1] Institute for Atmospheric and Earth System Research – INAR / Physics, P.O. Box 64, FI-00014 University of Helsinki, Finland.

[2] Aarhus University, Department of Chemistry, Langelandsgade 140, DK-8000 Aarhus C, Denmark.

[3] Aarhus University, Department of Physics and Astronomy, Ny Munkegade 120, DK-8000 Aarhus C, Denmark.

[4] Lund University, Division of Nuclear Physics, P.O. Box 118, SE-22100 Lund, Sweden.

[5] Aarhus University, Department of Environmental Science – Atmospheric Chemistry and Physics, Frederiksborgvej 399, DK-4000 Roskilde, Denmark.

[*] Presently at University of California, Department of Environmental Science, Policy and Management, Hilgard Hall 251B, CA-94720-3114 Berkeley, United States of America.

Correspondence to Lauriane L. J. QUÉLÉVER (Lauriane.quelever@helsinki.fi) & Mikael EHN (Mikael.ehn@helsinki.fi)

Abstract

Highly-oxygenated organic molecules (HOM) are important contributors to Secondary Organic Aerosol (SOA) and New-Particle Formation (NPF) in the boreal atmosphere. This newly discovered class of molecules is efficiently formed from atmospheric oxidation of biogenic volatile organic compounds (VOC), such as monoterpenes, through a process called autoxidation. This process, in which peroxy-radical intermediates isomerize to allow addition of molecular oxygen, is expected to be highly temperature-dependent. Here, we studied the dynamics of HOM formation during α-pinene ozonolysis experiments performed at three different temperatures, 20 °C, 0 °C and -15 °C, in the Aarhus University Research on Aerosol (AURA) chamber. We found that the HOM formation, under our experimental conditions (50 ppb α-pinene, 100 ppb ozone), decreased considerably as temperature decreased, with molar yields dropping by around a factor of 50 when experiments were performed at 0 °C, compared to 20 °C. At -15 °C, the HOM signals were already close to the detection limit of the nitrate-based Chemical Ionization Atmospheric Pressure interface Time Of Flight (CI-APi-TOF) mass spectrometer used for measuring gas-phase HOM. Surprisingly, very little difference was seen in the mass spectral distribution of the HOM molecules of interest at 0 °C and 20 °C, with e.g. the ratios between the typical HOM products $C_{10}H_{14}O_7$, $C_{10}H_{14}O_9$, and $C_{10}H_{14}O_{11}$ remaining fairly constant. The more oxidized species have undergone more isomerization steps, yet, at lower temperature, they did not decrease more than the less oxidized species. One possible explanation is be that the rate-limiting step forming these HOM occurs before the products become oxygenated enough to be detected by our CI-APi-TOF (i.e. typically seven or more oxygen atoms). The strong temperature dependence of HOM formation was observed under temperatures highly relevant for the boreal forest, but the exact magnitude of this effect in the atmosphere will be much more complex: the fate of peroxy-radicals is a competition between autoxidation (influenced by temperature and VOC type) and bimolecular termination pathways (influenced mainly by concentration of reaction

492 partners). While the temperature influence is likely smaller in the boreal atmosphere than in our
493 chamber, the magnitude and complexity of this effect clearly deserves more consideration in future
494 studies in order to estimate the ultimate role of HOM on SOA and NPF under different atmospheric
495 conditions.
496
497 **Keywords:** HOM formation & yield, Temperature, ACCHA campaign, AURA chamber, Mass
498 Spectrometry, CI-APi-TOF
499

500 1. Introduction

501
502 Aerosol particles impact Earth's climate by scattering and absorbing solar radiation, and by
503 influencing cloud properties when they act as Cloud Condensation Nuclei (CCN) (IPCC, 2013).
504 Organic compounds contribute significantly to the chemical composition of aerosol, accounting from
505 20 % to 90 % of the total aerosol mass of sub-micrometer particles depending on their location in the
506 globe (Jimenez et al., 2009). Submicron organic aerosol are dominantly secondary. Called Secondary
507 Organic Aerosol (SOA), they originate from gas-to-particle conversion from condensable vapors
508 (Hallquist et al., 2009; Zhang et al., 2007). These vapors are mainly oxidation products of Volatile
509 Organic Compounds (VOC), having sufficiently low vapor pressure (i.e. volatility) to condense onto
510 aerosol particles (Hallquist et al., 2009).
511
512 In order to interact efficiently with solar radiation or to activate cloud droplets, aerosol particles need
513 to be around 100 nm in diameter or larger (Dusek et al., 2006). If particles have formed through
514 nucleation processes in the atmosphere (e.g. Kulmala et al., 2013), their ability to grow to climate-
515 relevant sizes before being scavenged through coagulation is critically impacted by the rate at which
516 low-volatile vapors will condense onto them (Donahue et al., 2013). Extremely Low-Volatile Organic

517 Compounds (ELVOC), introduced by Donahue et al. (2012), have the ability to condense irreversibly
518 onto even the smallest aerosol particles and clusters and thus contribute to particle growth. Low-
519 Volatile Organic Compounds (LVOC), typically more abundant in the atmosphere, are important for
520 the growth of particles larger than a few nanometers (Tröstl et al., 2016).
521
522 Highly-oxygenated Organic Molecules (HOM, Ehn et al., 2014 & 2017; Bianchi et al., 2019) were
523 recently identified as a large contributor to (E)LVOC and the growth of newly formed particles (Ehn
524 et al., 2014; Tröstl et al., 2016). First observed in measurements of naturally charged ions in the boreal
525 forest (Ehn et al., 2010 & 2012) using the Atmospheric Pressure interface Time Of Flight (APi-TOF)
526 mass spectrometer (Junninen et al., 2010), HOM quantification only became possible through the
527 application of nitrate ion chemical ionization (CI) mass spectrometry (Zhao et al., 2013; Ehn et al.,
528 2014). Most studies have utilized the APi-TOF coupled to such a chemical ionization source (CI-
529 APi-TOF, Jokinen et al., 2012), and detailed laboratory studies have been able to elucidate the
530 primary formation pathways of HOM (Rissanen et al., 2014; Jokinen et al., 2014; Mentel et al., 2015).
531 We also note that the HOM-related terminology has evolved over the last years, and here we define
532 HOM as organic molecules formed through gas-phase autoxidation, containing six or more oxygen
533 atoms.
534
535 The main process in HOM formation is peroxy-radical (RO_2) autoxidation (Crounse et al., 2013),
536 which involves an intramolecular H-abstraction by the peroxy-radical group to form a hydroperoxide
537 and a carbon-centered radical to which molecular oxygen (O_2) can rapidly add to form a new RO_2
538 with a higher level of oxygenation. The efficiency of this process is mainly determined by the
539 availability of easily "abstractable" H-atoms, and such are often formed in the ozonolysis of
540 endocyclic alkenes (Rissanen et al., 2014 & 2015; Berndt et al., 2015). This structural component can
541 be found in many biogenic VOC, such as monoterpenes, enhancing their roles as SOA precursors

542 through efficient autoxidation and HOM formation (Ehn et al., 2014; Jokinen et al., 2014; Berndt et
543 al., 2016). Peroxy-radicals are important intermediates in nearly all atmospheric oxidation processes.
544 The RO_2 that have undergone autoxidation will terminate to closed-shell species in similar ways as
545 less oxidized RO_2, taking place either by unimolecular processes leading to loss of OH or HO_2, or
546 bimolecular reactions with NO, HO_2 or other RO_2. The termination pathway strongly influences the
547 type of HOM that can be formed, with e.g. $RO_2 + RO_2$ reactions being able to form ROOR dimers
548 and RO_2+NO often forming organic nitrates (Ehn et al., 2014; Berndt et al., 2018). All these
549 bimolecular reactions of peroxy-radicals, as well as the initial oxidant-VOC reaction, are temperature-
550 dependent. For example, the reaction rate of ozone with α-pinene, a broadly studied SOA-forming
551 system, is $6.2 \cdot 10^{17}$ ($\pm 1.3 \cdot 10^{17}$) cm^3 $molec^{-1}$ s^{-1} at 3 °C, and $8.3 \cdot 10^{17}$ ($\pm 1.3 \cdot 10^{17}$) cm^3 $molec^{-1}$ s^{-1}
552 at 22 °C (Atkinson et al., 1982). However, the intramolecular isomerization through H-shifts is likely
553 to have a much stronger temperature dependence, due to the higher energy barrier for the H-shift
554 (Seinfeld and Pandis, 2006; Otkjær et al., 2018). As an example (Praske et al., 2018) reported
555 theoretical estimates of different H-shifts in hexane-derived RO_2 which increased roughly by a factor
556 of 5 to10 when the temperature increases by 22 °C (from 23 °C to 45 °C). Possible changes in HOM
557 formation as a function of temperature are thus expected to derive mainly from changes in the
558 autoxidation process. However, a detailed mechanistic understanding the various autoxidation steps,
559 let alone their temperature dependencies, is still lacking for most atmospheric VOC-oxidant systems,
560 owing partly to the plethora and the complexity of the possible reaction pathways.
561
562 Despite recent work in determining the impact of temperature on aerosol formation (Kristensen et al.,
563 2017; Stolzenburg et al., 2018), literature on corresponding HOM effects are extremely limited. At
564 room temperature (i.e. 20 ±5 °C), HOM molar yields have been estimated to be some percent for
565 most monoterpenes in reactions with ozone or OH (Ehn et al., 2014; Jokinen et al., 2015). Only very
566 recently, studies were presented where HOM formation experiments have been conducted at varying

567 temperatures. Stolzenburg et al. (2018) showed that at lower temperatures, the CI-APi-TOF detects
568 much lower HOM concentrations, though no quantitative values on the HOM yields were given. The
569 impact of decreased HOM on new-particle growth rates was compensated by less oxidized species
570 being able to condense at the lower temperatures. In another study, Frege et al. (2018) also concluded
571 that HOM formation decreased at lower temperatures, but their study was based on observations of
572 naturally charged ions using an APi-TOF, complicating the interpretation of HOM formation rates.
573
574 In this study, we directly evaluate the impact of temperature on HOM yields in a laboratory chamber
575 during α-pinene ozonolysis experiments at 20 °C, 0 °C and -15 °C. Relative changes in HOM
576 formation are compared between temperatures both for total HOM yields as well as on a molecule-
577 by-molecule basis. The more detailed impact of temperature on the molecular distribution of HOM
578 is expected to provide new insights into critical steps in the formation pathways.
579

580 # 2. Methods

581

582 ## 2.1. The AURA Chamber

583 A detailed description of the AURA chamber can be found in Kristensen et al. (2017). Essentially, it
584 consists of a 5 m^3 Teflon® bag contained in a temperature-controlled enclosure. Configured in batch
585 sampling mode, the chamber was initially cleaned by flushing at 20 °C with purified ambient air (i.e.
586 filtered air exempt of particles, water vapor and VOC, and reduced NOx concentration), and
587 subsequently set to the desired temperature and finally filled with the necessary reagents. Over the
588 course of the experiment, it was progressively emptied due to sampling by the measuring
589 instrumentation. In our experiments, we first added ozone to a concentration of 100 ppb, provided by
590 an ozone generator (Model 610, Jelight Company, Inc.) after which the oxidation reaction started when

591 the VOC was introduced by vaporization of a calculated volume of liquid reagent (α-pinene or β-
592 pinene) into a hot stream of nitrogen, reaching the desired VOC concentration (10 or 50 ppb).
593
594 **2.2. The ACCHA Experiment**
595 The Aarhus Chamber Campaign on HOM and Aerosols (ACCHA) experiment aimed to explore
596 oxidation processes and aerosol formation during dark monoterpene ozonolysis at different
597 temperatures, from -15 °C to 20 °C. The experiments focused on α-pinene oxidation at two different
598 concentrations (10 ppb and 50 ppb) for three different temperatures: -15 °C, 0 °C and 20 °C. Two
599 additional experiments were conducted with temperatures ramped from the coldest to the warmest or
600 reversely during experiments at 10 ppb of α-pinene. For comparison, fixed temperature runs were
601 also performed using β-pinene, at a concentration of 50 ppb. Ozone (100 ppb) was used as the main
602 oxidant, but hydroxyl radicals also took part in the oxidation reactions as OH-scavengers were not
603 employed in the experiments discussed here. According to model simulations using the master
604 chemical mechanism v3.3.1 (Jenkin et al., 1997 & 2015; Saunders et al., 2003), ozonolysis accounted
605 for approximately 2/3 and OH-oxidation for 1/3 of the α-pinene oxidation respectively. A table
606 summarizing the experiments of the campaign can be found in the Appendix (Table A1).
607
608 **2.3. Instrumentation**
609 The ACCHA experiment involved a diverse set of instruments measuring both the gas phase and the
610 particle phase. The gas phase instrumentation included a Proton Transfer Reaction Time Of Fight
611 Mass Spectrometer (PTR-TOF-MS, Model 8000-783, IONICON Inc., Jordan et al., 2009) for
612 measuring the concentrations of the injected VOCs and other volatile products, as well as a nitrate-
613 based Chemical Ionization Atmospheric Pressure interface Time of Flight (CI-APi-TOF, TOFWERK
614 A.G. & Aerodyne Research Inc., Jokinen et al., 2012) mass spectrometer, analyzing the highly
615 oxidized organic products of lower volatility (e.g. HOM). The CI-APi-TOF is described in more

616 detail in the following section. The aerosol phase measurement was done using (1) a nano-
617 Condensation Nuclei Counter (nCNC), being a combination of a Particle Size Magnifier (PSM,
618 Model A10, Airmodus Ltd.) and a Condensation Particle Counter (CPC, Model A20, Airmodus Ltd.),
619 (2) a Scanning Mobility Particle Sizer (SMPS; Kr-85 neutralizer (Model 3077A, TSI), electrostatic
620 classifier (Model 3082, TSI), nano-water-based CPC (Model 3788, TSI)), counting the size resolved
621 particles from 10 nm to 400 nm, (3) a High Resolution Time-Of-Flight Aerosol Mass Spectrometer
622 (HR-TOF-AMS, Aerodyne Research Inc., Jayne et al., 2000) determining the chemical composition
623 of non-refractory aerosol particles larger than ~35 nm. The temperature and relative humidity inside
624 the chamber were monitored using HC02-04 sensors (HygroFlex HF320, Rotronic AG), and the
625 ozone concentration was measured with an ozone monitor (O_3-42 Module, Environment S.A.).
626
627 **2.4. Measuring highly oxygenated organic molecules in the gas phase**
628 HOM present in the gas phase were measured using a CI-APi-TOF mass spectrometer. The
629 instrument sampled air at about 80 cm from the wall of the chamber via a ¾ inch tube directly
630 connected to the CI-APi-TOF, which was located outside the chamber enclosure (~20 °C at all time).
631 The sheath air (taken from a compressed air line) was 30 LPM and the total flow (generated by the
632 house vacuum line) was 40 LPM. The ~1 m long inlet had a flow of 10 LPM caused by the difference
633 between the sheath and total flows. With such a tube length and flow, roughly half of the HOM are
634 expected to be lost to the walls of the inlet lines. The CI-APi-TOF is described by Jokinen et al.
635 (2012), but also briefly presented here. Strong acids and highly oxygenated organic molecules have
636 been shown to cluster efficiently with nitrate ion (Ehn et al., 2014; Hyttinen et al., 2015). Nitrate ions
637 (i.e. NO_3^-, $HNO_3NO_3^-$ and $(HNO_3)_2NO_3^-$), produced by exposure of nitric acid vapors to soft X-ray
638 radiation, were electrostatically introduced into the sample flow of 10 LPM with a reaction time of
639 roughly 200 ms at atmospheric pressure.

The ions, clusters with NO_3^-, were sampled through a 300 µm critical orifice into the APi, where ions were guided and focused by two segmented quadrupoles through chambers with gradually decreasing pressures (~2 mbar and ~10^{-2} mbar, respectively). Finally, an ion lens assembly, at ~10^{-5} mbar, guided the ions into the TOF chamber (~10^{-6} mbar) where they were orthogonally extracted and their mass-to-charge ratios determined. The detected signal of each ion is then expressed as counts per second (cps) or counts per second normalized by the sum of reagent (nitrate) ions (norm. cps). More detail about the APi-TOF itself can be found in Junninen et al. (2010). Quantification of HOM remains challenging, and, in this work, we aim at explaining the relative changes of HOM measured at different temperature rather than focusing on their absolute concentration. However, in some instances, we also estimate absolute quantities by applying a calibration factor C = 1.65 · 10^9 molecules cm^{-3}, (cf. Jokinen et al., 2012, for details on C). This translates to ~70 ppt of HOM per normalized counts. As no calibrations were performed during the ACCHA experiments, the value was taken from a sulfuric acid calibration (methodology according to Kürten et al., 2012) performed during an earlier measurement campaign. While associated with a large uncertainty (estimated to be at least -50 % / +100 %) using this value, we obtained HOM molar yields (as described in later sections) of a similar range as earlier studies (Jokinen et al., 2012; Ehn et al., 2014). We estimated a detection limit from our experimental data at the lowest temperature to be roughly 10^{-5} normalized counts, which correspond to ~10^4 molecules cm^{-3}.

2.5. HOM dynamics in a batch mode chamber

Being configured in batch mode, without active mixing, the AURA chamber is a dynamic reactor where concentrations of products are a function of cumulative sources and cumulative sinks from the start of the experiment. In the case of HOM, their lifetime in the gas phase must be short due to their low vapor pressure and, thus, their fast condensation. This means that the measured HOM

concentrations are mainly the result of production and loss having occurred within the previous minutes, as described in more detail in the following section.

The temporal change in HOM concentrations (i.e. $\frac{d[HOM]}{dt}$) can be expressed as the sum of the production terms and loss terms. The HOM formation is governed by the VOC reaction rate while the loss is dominated by condensation onto particles or walls. For the yield estimation analysis, we focus mainly on the high concentration experiments (i.e. [α-pinene] = 50 ppb), where the high condensation sink (CS, on the order of 0.1 s^{-1}) will dominate over the wall loss rate. In a smaller chamber with active mixing, the wall loss rate for low-volatile species has been estimated to be around 10^{-2} s^{-1} (Ehn et al., 2014), and in the AURA chamber we expect it to be much slower, likely on the order of 10^{-3} s^{-1}. Therefore, we can formulate simplified expression as in the following equations:

$$\frac{d[HOM]}{dt} = \gamma_{HOM} \cdot k \cdot [VOC] \cdot [O_3] - CS \cdot [HOM] \qquad (Eq.\,1)$$

$$\gamma_{HOM} = \frac{\frac{d[HOM]}{dt} + CS \cdot [HOM]}{k \cdot [VOC] \cdot [O_3]} \qquad (Eq.\,2)$$

Herein, γ_{HOM} corresponds to the HOM yield. The temperature-dependent rate constant of α-pinene ozonolysis, k, was taken to be $8.05 \cdot 10^{-16}$ $e^{-640/(273.15+T)}$ cm^3 $molecules^{-1}$ s^{-1}, where T is the temperature in degrees Celsius, (Atkinson, 2000; Calvert et al., 2002). Since the majority of HOM are irreversibly lost upon contact with a surface (Ehn et al., 2014), the CS represents the total sink at a time t. The CS was estimated using the measured particle number size distributions from the SMPS (Dal Maso et al., 2005). The molecular properties that govern the CS are the mass accommodation coefficient, the molecular diffusion coefficient and the mean molecular speed. Based on the work by Julin et al. (2014), the mass accommodation coefficient was set to unity. The molecular diffusion coefficient

was calculated using Fuller's method (Tang et al., 2015) and the mean molecular speed was calculated using kinetic theory. Both the molecular diffusion and speed depends on molecular composition and on the absolute temperature during the experiments. $C_{10}H_{16}O_7$ was taken as a reference for the CS estimation, being one of the most abundant HOM. In comparison, the CS calculated for the largest molecules (i.e. HOM dimers) were approximately 30 % lower. With the aforementioned assumptions, a distinct yield for each identified HOM of interest can be derived based on Eq. 2, as the slope of a linear fit to the data during an experiment, with $k \cdot [VOC] \cdot [O_3]$ on the x-axis and $\frac{d[HOM]}{dt} + CS \cdot [HOM]$ on the y-axis.

3. Results & Discussion

3.1. Effect of the temperature on the CI-APi-TOF

Since this work targets the variation of HOM in relation to temperature, it is necessary to assess the reliability of the CI-APi-TOF measurement towards temperature variations. The sensitivity towards a certain molecule depends to first approximation on the charging efficiency in the CI inlet and the transmission efficiency of the sampled ion in the APi-TOF. The charging efficiency of a HOM is primarily determined by the stability of the HOM · NO_3- cluster relative to the HNO3 · NO_3- cluster (Hyttinen et al., 2015), and we do not expect temperature to cause a large difference in this relative behavior. However, the transmission can be sensitive to small changes, and especially pressures inside the instrument are important to monitor, as the optimal voltages guiding the sampled ions through the instrument have been tuned for specific pressures. The pressures of the two quadrupole chambers (named "SSQ" and "BSQ", respectively, where the pressure dependence is the largest) as well the Total Ion Count (TIC, i.e. sum of all signals), the Reagent Ion Count (RIC, i.e. sum of nitrate ion signals) and the contributions of each nitrate ion signals are presented in Figure 1. The SSQ

713 pressures (Fig. 1a) were found relatively stable (average: ~2.07 mbar) and the BSQ averaged pressure
714 (Fig. 1b) was ~$3.3 \cdot 10^{-2}$ mbar, which are typical values for this instrument. Unfortunately, the other
715 instrumental pressures (i.e. ion lens assembly chamber or TOF chamber pressures) were not recorded
716 due to sensor failures. However, as these chambers are at low enough pressures that ion-gas collisions
717 are very rare, any possible small variations in the pressures are unlikely to affect our results. When
718 going from the coldest temperature (-15 °C) to the highest (20 °C), in a continuous temperature ramp,
719 the SSQ pressure decreased by ~0.01 mbar, corresponding to a relative change of 0.5 % (Fig. 1a).
720 Over the same temperature range, the pressure within the second chamber (BSQ) decreased by ~1.5
721 $\cdot 10^{-3}$ mbar (~4.5 %) when the temperature varied by 35 °C (Fig. 1a). The same characteristics were
722 observed when comparing across experiments performed at constant temperatures and for the
723 continuous temperature ramping experiments. The SSQ pressure values below 2.02 mbar at -15 °C
724 and 20 °C, corresponding also to the lowest BSQ pressures measured, were related to particularly
725 low ambient pressures (~981.8 mbar). Thus, the effect of temperature within the AURA chamber
726 caused smaller variability of the internal pressures than ambient pressure changes.
727

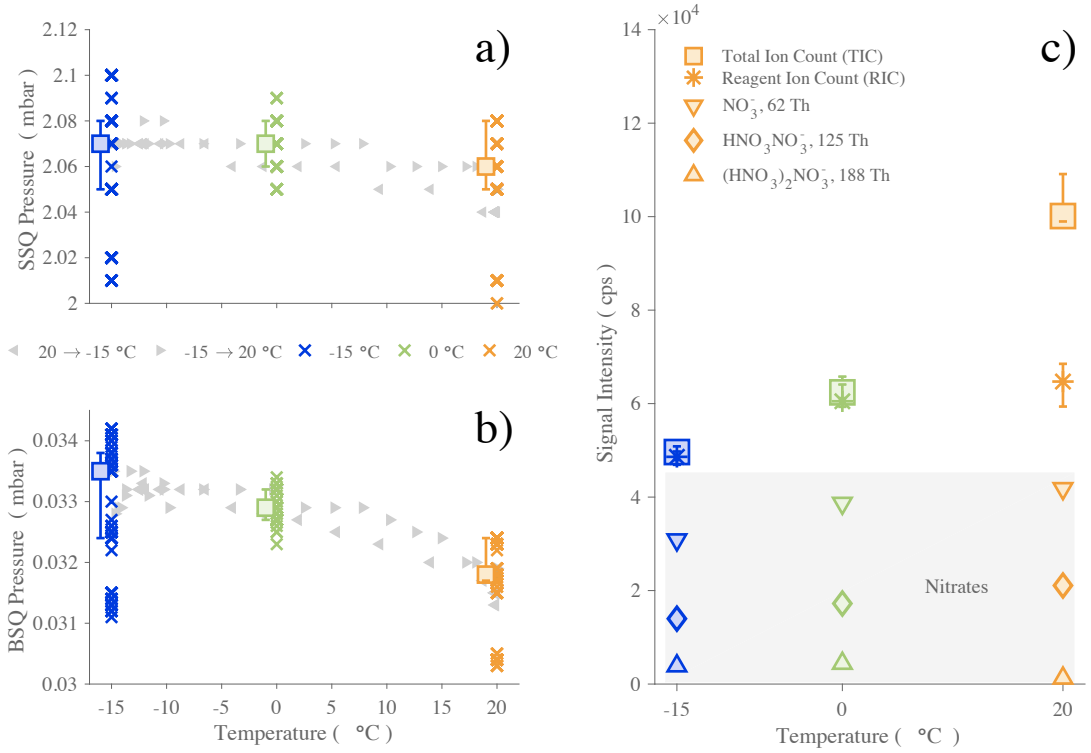

Figure 1: Evolution of the CI-APi-TOF pressures in the first (a) and second (b) quadrupole chambers (SSQ and BSQ, respectively) and signal counts (c) as a function of temperature in the AURA chamber. The APi pressures (panels a & b) are represented by crosses, depicting 10-minute averaged data points for all α-pinene ozonolysis experiments, colored by temperature (blue for -15 °C, green for 0 °C and orange for 20 °C). The squares are the median values for each temperature with their 75th and 25th percentiles. Additionally, the gray triangles relate the data (10-minute averages) of two temperature ramp experiments, from -15 °C to 20 °C (right-pointing triangles) or from 20 °C to -15 °C (left-pointing triangles). Panel c) shows averages of the sum of all ion signals (TIC, square-markers) and the sum of all reagent ion signal (RIC, asterisks-markers). RIC markers also include 25th and 75th percentiles. Nitrate signal contributions are also included separately (markers in gray-shaded area: down pointing triangle for NO_3^-, diamond marker for $HNO_3NO_3^-$ and triangle pointing upward for $(HNO_3)_2NO_3^-$).

The RIC signal (Fig. 1c) stayed within the range 5-7 · 10^4 cps, with its lowest values observed at -15 °C. The comparatively larger increase in TIC at the highest temperature is mainly explained by the fact that much higher HOM concentrations were formed at 20 °C compared to lower temperature

744 experiments, and the transmission at these masses is generally higher than in the region of the reagent
745 ions (Junninen et al., 2010; Ehn et al., 2011; Heinritzi et al., 2016). We conclude from the above
746 investigations that changes on the order of tens of percent, based on the variation in RIC,
747 occurred in our instrument as the AURA chamber temperature was varied, and that only signal
748 changes larger than this should be attributed to actual perturbations in the chemistry taking
749 place in the chamber.
750
751 **3.2. Ozonolysis reaction in the AURA chamber: a typical α-pinene experiment at 20 °C**
752 Selected gas phase precursors and products, including aerosols, for a high-load (i.e. 50 ppb, during
753 12-Jan-2017) α-pinene oxidation experiment at 20 °C are shown in Figure 2. The steep increase in α-
754 pinene concentration, measured by PTR-TOF-MS, indicates the start (defined as time 0) of the
755 oxidation reaction experiment (Fig. 2a). The formed aerosol product, i.e. particle number and aerosol
756 mass, are presented in Fig. 2c. Herein, we observe an increase of the aerosol mass over the first two
757 hours of the experiment whereas the particle number concentration plateaued in the first ten minutes
758 after VOC injection. On the other hand, the HOM signals (Fig. 2b) show a large increase immediately
759 as the VOC was injected. A smaller increase was also observed when the ozone was introduced, most
760 likely due to residual volatiles reacting with ozone inside the chamber. After the first 10 min, HOM
761 signals start to decrease as the CS (Fig. 2d) rapidly increases under these high aerosol loads. After
762 the first half hour, the CS only changes by some tens of percent, while the VOC oxidation rate (gray
763 crosses in Fig. 2b) decreases around one order of magnitude over the following hours of the
764 experiment. Therefore, concentrations of low-volatile HOM should largely track the decay rate of the
765 VOC oxidation rate, which is also observed. We observe a slower decay of HOM monomers than
766 dimers, suggesting that some of the monomers may be semi-volatile enough to not condense
767 irreversibly upon every collision with a surface, and/or that the VOC oxidation rate also influences
768 the formation chemistry, as discussed in more detail in later sections.

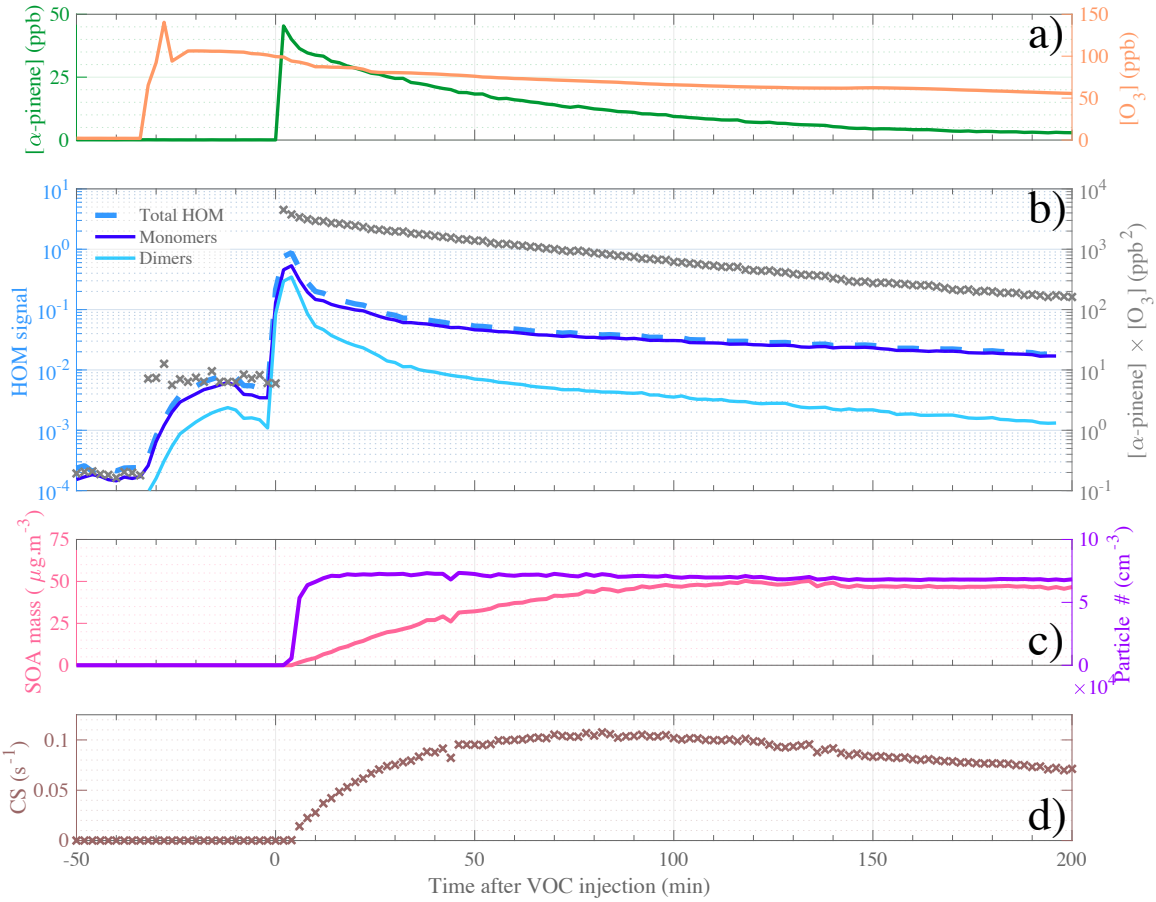

Figure 2: Temporal evolution of the main parameters during a typical α-pinene ozonolysis experiment (initial conditions: [α-pinene] = 50 ppb, [O_3] = 100 ppb, T = 20 °C). Reactant concentrations are shown in Panel a, with α-pinene concentration in dark green and ozone concentration in orange. HOM signals are plotted in Panel b, with a distinction between Total HOM (dashed medium-blue line), HOM monomers ($C_{10}H_{14-16}O_{7-11}$, dark blue line) and HOM dimers ($C_{19-20}H_{28-32}O_{10-18}$ light blue line), as well as the product [α-pinene] · [O_3] represented by gray cross markers. Panel c depicts the SOA mass (pink line) and the particle concentration (purple line). Panel d shows the evolution of the condensation sink. The time span (in x-axis) is expressed as minutes after α-pinene injection, thus the time zero represents the start of the experiment.

For a more detailed investigation at the HOM formation upon the reaction between ozone and α-pinene, we compare compounds observed in the range between 300 – 600 Thomson (Th) in the CI-APi-TOF, during a background measurement before and 10 min after α-pinene injection for each

temperature (Figure 3). The largest HOM signals, highlighted in darker colors, are primarily observed at the highest temperature, but also in the monomer area (300 – 375 Th). The dimer signals (between 450 – 600 Th) are smaller, but still contribute significantly to the total HOM concentration. With the exception of the -15 °C experiment where HOM dimers already reach the background level after 10 min, all molecules selected as representative HOM are present in all the spectra. The detailed peak list of HOM compounds, selected for their high signal intensity, including exact masses and elemental composition is provided in the Appendix (Table A2).

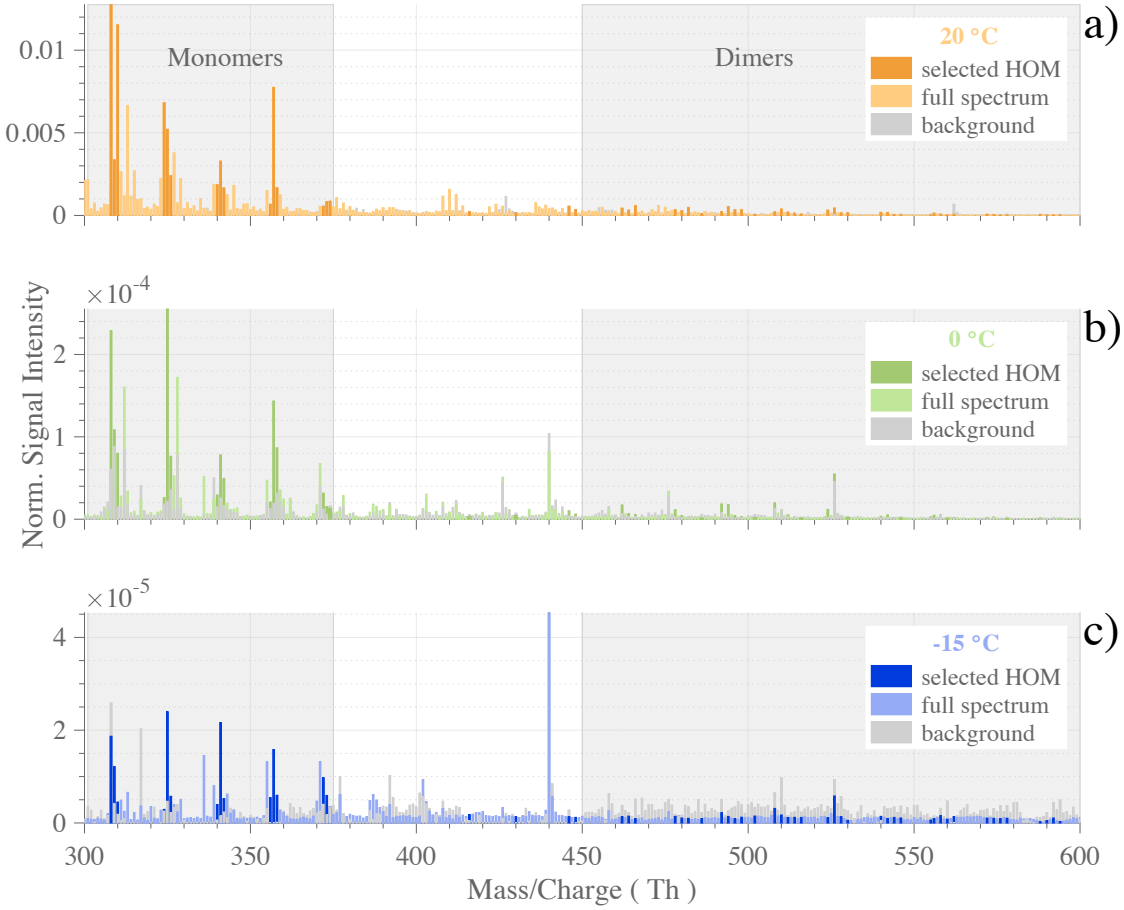

Figure 3: Typical HOM mass spectra observed during α-pinene ozonolysis experiments (initial conditions: [α-pinene] = 50 ppb, [O3] = 100 ppb,) at T = 20 °C (panel a) in orange, T = 0 °C (panel b) in green, T = -15 °C

(panel c) in blue. The normalized signals were averaged over 5 minutes during background measurement before VOC injection (gray bars), and from 40 min to 120 min after α-pinene injection (colored bars). Specific masses, selected for representing high-intensity HOM, are highlighted in darker colors. Gray-shaded areas show HOM sub-ranges of monomers and dimers.

3.3. Effect of the temperature on measured HOM

We performed a total of twelve α-pinene ozonolysis experiments with seven at high loading (i.e. [α-pinene] = 50 ppb), out of which two were conducted at 20 °C, two at 0 °C and three at -15 °C. Three experiments were performed with [α-pinene] = 10 ppb – one for each aforementioned temperature. Experiments with 50 ppb of β-pinene were also performed at the same three temperatures (see Table A2). An overview of HOM measurements for the different experiments is shown in Figure 4, with distinction between HOM monomers (Fig. 4a) and dimers (Fig4. b) as defined earlier.

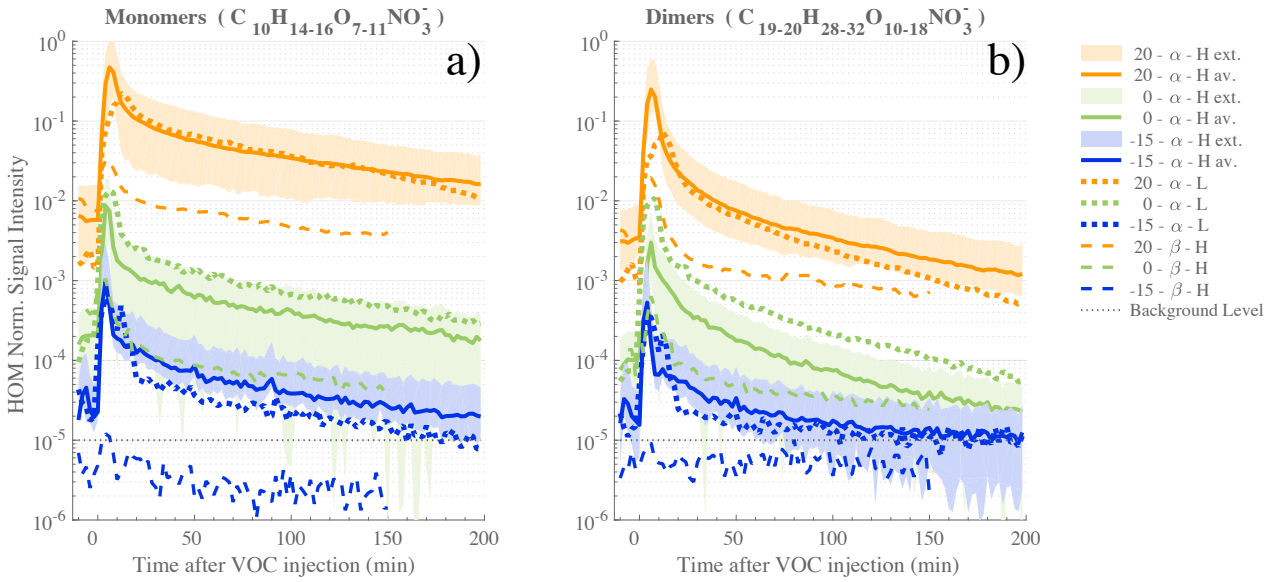

Figure 4: Time series of HOM measured during the ACCHA campaign. HOM monomer (a) and dimer (b) traces include compounds with a chemical composition of $C_{10}H_{14\text{-}16}O_{7\text{-}11}$ and $C_{19\text{-}20}H_{28\text{-}32}O_{10\text{-}18}$, respectively. The series are colored based on temperature, orange for 20 °C experiments, green for 0 °C and blue for -15 °C. Statistics over α-pinene ("α" in the

legend) high load (50 ppb, "H") experiments are shown, with averaged values ("av." in continuous line) and the maximum and minimum values of the measured HOM signal (bounded shaded area). α-pinene low load (L) experiments are symbolized with colored dotted lines and the β-pinene ("β") experiments by dashed lines. The gray dotted line depicts the estimated background level of the CI-APi-TOF.

For a similar experiment type (i.e. same initial VOC concentrations), it can be seen that the resulting HOM concentrations were considerably impacted by the temperature at which the oxidation reaction occurred. The signal intensity for HOM monomers from α-pinene measured 30 minutes after the VOC injection was roughly two orders of magnitudes higher at 20 °C compared to 0 °C, and about three orders of magnitude higher compared to the -15 °C experiment. Very similar behavior is observed with respect to temperature for the dimer species as well, but with the differences that (1) less dimers are found in comparison to the HOM monomers and (2) HOM dimer concentrations are found to decrease at a faster rate during the experiment. The faster decrease of dimers compared to monomers results either from a lower production or a higher loss for dimers towards the end of the experiments. We expect that the reduced [α-pinene] and [O_3], leading to slower oxidation rates and consequently lower [RO_2] will have a greater impact on the dimers than the monomers, as the formation rate of dimers is proportional to [RO_2]^2, while monomers can still be formed efficiently via other RO_2 termination pathways, as discussed earlier.

When comparing the high (50 ppb) and low (10 ppb) loading α-pinene experiments, HOM signals were within the same range of concentration, and even higher at 0 °C the HOM were even more abundant in the low initial VOC concentration. Although this result may seem surprising at first, it only verifies our assumptions in Eq. 1 that the HOM concentration is a relatively simple function of formation and loss rates. Despite the fact that the low-concentration experiments had five times lower [VOC] (and consequently five times lower HOM formation rate), the condensation sink, being the primary loss for HOM, was ~8 times due to reduced aerosol formation. In other words, the loss rates

decreased more than the formation rate when the precursor concentration was lowered, resulting in an increase of [HOM].

Finally, the use of β-pinene as HOM precursor produced significantly less HOM, with concentrations being more than a factor of 10 lower compared to experiments performed with α-pinene at the same conditions. This agrees with earlier studies (Jokinen et al., 2014; Ehn et al., 2014) which have shown clearly lower HOM yields for β-pinene compared to α-pinene ozonolysis. The difference is primarily attributed to the exocyclic double bond in β-pinene. Note that, the β-pinene HOM concentrations at the lowest temperature, -15 °C, were below the instrumental limit of detection.

3.4. Yield estimation and temperature influence for molecule-specific HOM

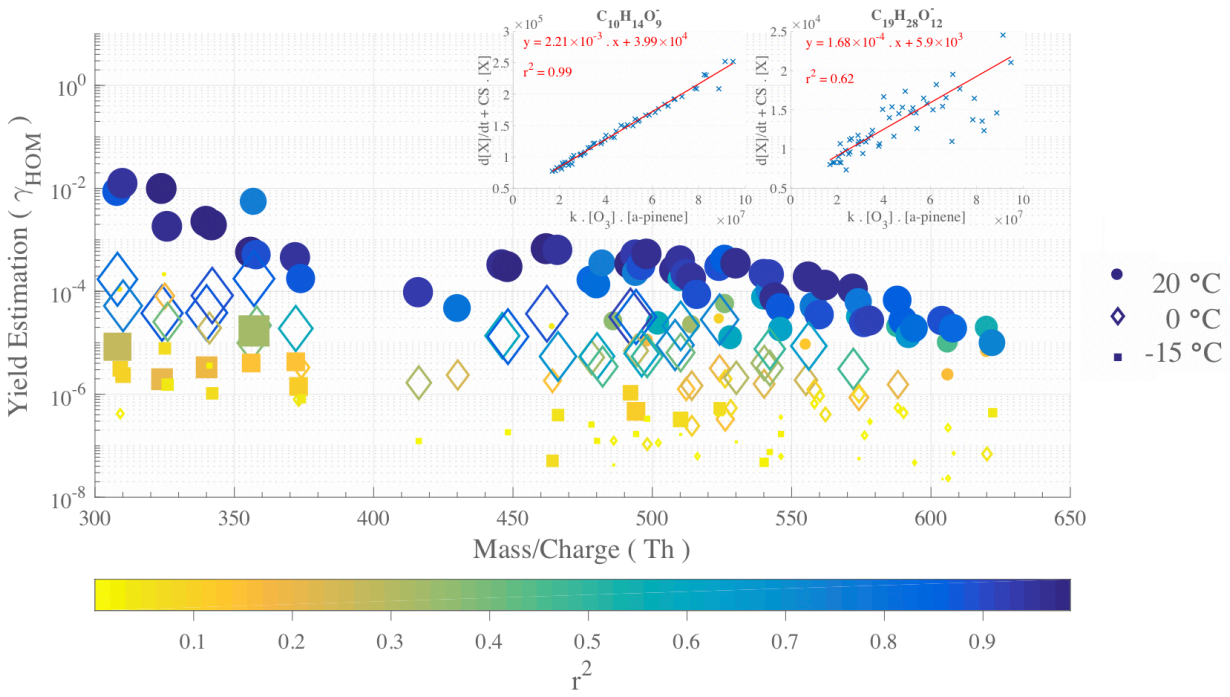

Figure 5: Yield estimations for individual α-pinene HOM from linear fits at 20 °C, 0 °C and -15 °C, from 40 to 120 min after α-pinene injection. Filled circles symbolize data from a 20 °C experiment (12-Jan-2017), diamond symbols illustrate 0 °C data (16-Jan-2017), and the filled squares represents -15 °C data (13-Jan-2017). The markers are colored and sized by r^2 values, coefficient of determination, evaluating the goodness of the linear fit

used to derive the yields. The top-right insets show two examples (for $C_{10}H_{14}O_9$ and $C_{19}H_{28}O_{12}$ at 20 °C) of the yield determination by robust linear fits to the variables described in the methods section.

We determined yield estimates, individually for each HOM of interest, from the results of a robust linear fit as described in the methods section and Eq. 2. We performed the fit with 2-min averaged data points from 40 min to 120 min after the VOC injection. The yield results are shown in Figure 5, with fit examples shown for $C_{10}H_{14}O_9$ and $C_{19}H_{28}O_{12}$ in the insets. As expected, based on Figure 4, the retrieved yield values (γ_{HOM}) decrease considerably with colder reaction conditions, with a total HOM yield (i.e. sum of the individual yields for each temperature) found to be 5.2 % at 20 °C, 0.10 % at 0 °C and $6.3 \cdot 10^{-3}$ % at -15 °C.

We again emphasize the large uncertainties in these molar yield estimations, but the HOM yield values for T = 20 °C does agree well with earlier reported values (e.g. Ehn et al. (2014), Jokinen et al. (2014), Sarnela et al. (2018)). As the largest contribution to the HOM yield comes from the least oxidized monomers (e.g. high signal intensity at 308 Th and 310 Th for $C_{10}H_{14}O_7$ and $C_{10}H_{16}O_7$ respectively), the molar yield may be slightly over-estimated, especially at 20 °C, due to the loss rates possibly being lower than assumed if these HOM are not condensing irreversibly onto the aerosol. γ_{HOM} values are on average higher for HOM monomers than for dimers, with the overall shape of the distribution closely resembling the mass spectrum in Figure 3. We performed the same calculation for the experiment were [α-pinene] = 10 ppb and found total HOM-yields in the same range, as the numbers found at 50 ppb, considering our estimated uncertainty: 8.8 % at 20 °C, 0.25 % at 0 °C and $5.5 \cdot 10^{-3}$ % at -15 °C. The slightly higher values may indicate that at the higher loadings, bimolecular RO_2 termination reactions are already occurring so fast that autoxidation is hampered. The total HOM yield decrease when going from 20 °C to 0 °C decreased by a factor 50 at the higher loadings, while the corresponding value at lower loadings was 35.

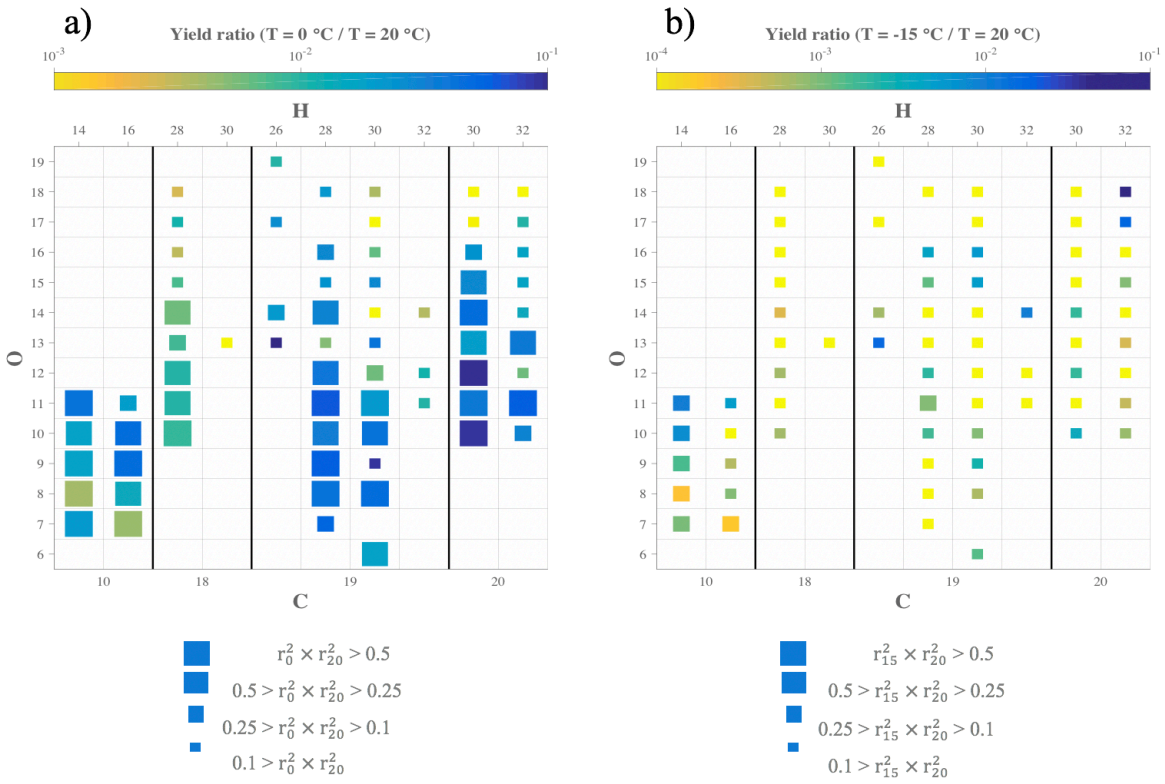

Figure 6: Comparison of yields for specific HOM compositions at different temperatures. Each square symbolizes a specific HOM measured by the CI-APi-TOF. The elemental composition can be read by taking the number of C atoms from the bottom axis, the number of H atoms from the top axis, and the number of O atoms from the left axis. The size of the square depicts the goodness of fit (r^2) used to derive the yields, and color shows the ratio of the yield at 0 °C (Panel a) or -15 °C (Panel b) compared to the yield measured at 20 °C.

While Figure 5 showed the estimated yields for every HOM at every temperature probed, specific chemical composition cannot be read from the plot. In order to assess the impact of temperature of the yield of HOM based on each elemental composition, Figure 6 depicts for each compound the ratio of the yield at 0 °C (Fig. 6a) or -15 °C (Fig. 6b) compared to the yield at 20 °C for a high load experiment of α-pinene ozonolysis. In Fig. 6a, many larger squares are observable, indicating a good reliability of our comparison analysis, but in Fig. 6b, it is clear that the HOM concentrations at the lowest temperature were too low to provide much reliable compound-specific information. From Fig. 6a we see no clear trend in the yield change for any column (i.e. changing oxygen content HOM with

a given amount of C and H). The HOM yields yield ratios between the two temperatures are primarily within 10^{-2} – 10^{-1}, meaning that the molecule-specific yields dropped to between 1-10 % when temperature decreased from 20 °C to 0 °C. If autoxidation of RO_2 decreased this considerably, one could have expected the more oxygenated HOM to decrease more than the less oxygenated ones. However, this did not seem to be the case, as e.g. some of the most abundant HOM $C_{10}H_{14}O_7$, $C_{10}H_{14}O_9$, and $C_{10}H_{14}O_{11}$ seemingly decreased the same amounts.

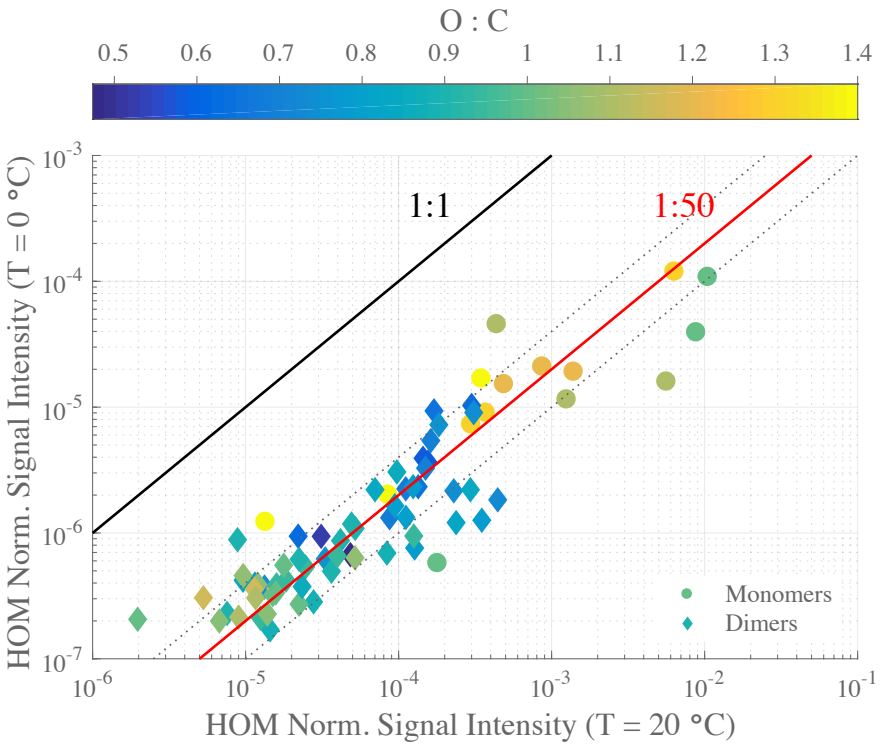

Figure 7: Scatter plot of HOM normalized signal intensity at 0°C and at 20 °C. The data points are colored by oxygen-to-carbon ratio with distinction between monomer – circle markers - and dimer compounds – diamond markers. Guide lines were added as indicators: 1:1 line – in black, 1:50 line – in red ,1:25 and 1:100 lines - in dotted grey.

In Figure 7, we show the HOM signal intensities, molecule by molecule based on the O:C ratio, from the 20 °C-experiment compared to the one at 0 °C. The vast majority of compounds fall close to the 1:50 line, which indicates similarities in the HOM spectra at both temperatures. Additionally, the

points with the largest scatter (e.g. >50 % from the 1:50-line) show no trends as a function of oxygen content, which also agrees with our observations from Figure 6. One possible interpretation of this is that the rate-limiting step in the autoxidation chain takes place in RO_2 radicals with 6 or less O atoms, which are not detected with our CI-APi-TOF, while the later H-shift reactions are fast enough that other reactions still do not become competitive. These "non-HOM" RO_2 radicals may then also be key molecules for determining the final branching leading to the different observed HOM with 7 or more O atoms. This may shed light on one of the main open challenges (Ehn et al., 2017) in understanding HOM formation, namely how RO_2 radicals with e.g. 6, 8 and 10 O atoms can form within a second, yet the relative distribution of these three does not change if the reaction time is allowed to increase (Berndt et al., 2015). Since the O_{10}-RO_2 (or its closed shell products) are not seen to accumulate over time, our results here provide support for a pathway where the O_6- and O_8-RO_2 are to some extent "terminal" products incapable of further fast H-shift reactions, while the O_{10}-RO_2 has been formed via another branch of the reaction where the autoxidation is able to proceed further. In this branch, the O_6- and O_8-RO_2 are likely only short-lived intermediates. While in no way conclusive, this highlights the need for fast measurements of HOM formation as well as improved techniques for observing less oxidized RO_2 radicals.

The only compound group where a slight decrease can be seen as a function of O-atom content is the $C_{20}H_{30}$ dimers. Interestingly, these also show some of the smallest yield ratios of all compounds. At the same time, the level of C_{18} dimers appears to drop most of all compound groups, potentially suggesting that the mechanism through which carbon atoms were lost on the way to the C_{18} dimers was sensitive to temperature, and at 0 °C the fragmentation was less prominent. It is conceivable that the different branching at 0 °C caused some of the C_{18} dimer precursors to form C_{20} dimers instead. However, this issue would need more detailed experiments in order to verify.

936 The decrease in HOM yield due to slower RO_2 H-shift rates at lower temperatures was found to be
937 very dramatic under our conditions. However, the exact magnitude of this decrease in HOM yield is
938 determined by the processes competing with the H-shifts. Under our conditions, the RO_2 lifetime is
939 kept quite short, both due to bimolecular ($RO_2 + RO_2$ or $RO_2 + HO_2$) reactions and collisions with
940 particles, and therefore any reduction in H-shift rates can strongly reduce the HOM yield. Inversely,
941 under very low loadings, the RO_2 lifetime may be long enough that the temperature decreases from
942 20 °C to 0 °C may cause much smaller changes in the HOM yields. If the lifetime of RO_2 radicals is
943 clearly longer than the time needed for multiple consecutive H-shifts to take place, HOM yields would
944 decrease only marginally with temperature. In the atmosphere, RO_2 lifetime will often be governed
945 by NO, which means that there can exist an intricate dependence of HOM yields as a function of
946 temperature, VOC type, VOC oxidation rate, and NO_X.

947

948 # 4. Conclusion

949

950 We present laboratory studies of HOM formation from monoterpene ozonolysis at different
951 temperatures (20 °C, 0 °C, and -15 °C). Our main insight is that temperature, in the studied range,
952 considerably impacted the HOM formation, decreasing the observed HOM yield by around 50-fold
953 upon a decrease by 20 °C. The exact temperature dependence of HOM formation in general is likely
954 both VOC- and loading-dependent, due to the competition between autoxidation and termination
955 reactions, and will likely be smaller at lower loadings. While autoxidation is expected to decrease
956 with temperature, our result is still striking as it takes place over a temperature range which is
957 atmospherically relevant for areas where monoterpene emissions are abundant, e.g. the boreal forest.
958 One important observation was that HOM were present at all measured temperatures with roughly
959 similar spectral distributions. This suggested that the total HOM yield as well as the final HOM
960 distribution are mainly determined by the first H-shift steps, i.e. in the region where the CI-APi-TOF

961 is unable to measure. This highlights the need for more comprehensive observations of autoxidation,
962 allowing direct observations of the critical steps determining the HOM yields and, subsequently, the
963 production rate of low-volatile organic compounds able to form secondary organic aerosol.
964

965 ## Authors Contribution

966

967 M. Ehn, M. Bilde, and M. Glasius supervised the ACCHA campaign. L.L.J Quéléver, K. Kristensen,
968 M. Bilde and M. Ehn designed the experiments. K. Kristensen and L. N. Jensen initialized the
969 chamber for experiments. L.L.J. Quéléver performed the measurement and analyzed the gas-phase
970 HOM. K. Kristensen and L. N. Jensen measured and analyzed the aerosol phase. K. Kristensen, B.
971 Rosati and R. Teiwes measured and analyzed the VOCs and their semi-volatile oxidation production,
972 also supervised by R. Bossi. M. Ehn, K. Daellenbach, O. Peräkylä and P. Roldin guided and helped
973 the analysis of HOM yield performed by L.L.J. Quéléver. L. L. J. Quéléver prepared the manuscript
974 with the contribution from all co-authors.
975

976 ## Acknowledgments

977

978 This work was funded by the European Research Council (Grant n°: 638703-COALA), the Academy
979 of Finland Center of Excellence program (Grant n°: 307331), Aarhus University and the Aarhus
980 University Research Foundation. We also thank H. Skov (Aarhus University, Department of
981 Environmental Science) for the use of the PTR-TOF-MS. We express our gratitude for the free use
982 of mass spectrometry analysis tools: TofTools freeware provided by H. Junninen. O. Peräkylä thanks
983 the Vilho, Yrjö & Kalle Väisälä Foundation. We also thank M. P. Rissanen and T. Kurtén for their
984 spontaneous input on this work.
985

References

Atkinson, R., Winer, A., and Pitts Jr, J.: Rate constants for the gas phase reactions of O3 with the natural hydrocarbons isoprene and α-and β-pinene, Atmospheric Environment (1967), 16, 1017-1020, 1982.

Atkinson, R.: Atmospheric chemistry of VOCs and NOx, Atmospheric environment, 34, 2063-2101, 2000.

Bianchi, F., Kurtén, T., Riva, M., Mohr, C., Rissanen, M. P., Roldin, P., Berndt, T., Crounse, J. D., Wennberg, P. O., and Mentel, T. F.: Highly Oxygenated Organic Molecules (HOM) from Gas-Phase Autoxidation Involving Peroxy Radicals: A Key Contributor to Atmospheric Aerosol, Chemical Reviews, 2019.

Berndt, T., Richters, S., Kaethner, R., Voigtländer, J., Stratmann, F., Sipilä, M., Kulmala, M., and Herrmann, H.: Gas-phase ozonolysis of cycloalkenes: formation of highly oxidized RO_2 radicals and their reactions with NO, NO2, SO2, and other RO_2 radicals, The Journal of Physical Chemistry A, 119, 10336-10348, 2015.

Berndt, T., Richters, S., Jokinen, T., Hyttinen, N., Kurtén, T., Otkjær, R. V., Kjaergaard, H. G., Stratmann, F., Herrmann, H., and Sipilä, M.: Hydroxyl radical-induced formation of highly oxidized organic compounds, Nature communications, 7, 13677, 2016.

Berndt, T., Scholz, W., Mentler, B., Fischer, L., Herrmann, H., Kulmala, M., and Hansel, A.: Accretion Product Formation from Self-and Cross-Reactions of RO_2 Radicals in the Atmosphere, Angewandte Chemie International Edition, 57, 3820-3824, 2018.

Calvert, J. G., Atkinson, R., Becker, K. H., Kamens, R. M., Seinfeld, J. H., Wallington, T. H., and Yarwood, G.: The mechanisms of atmospheric oxidation of the aromatic hydrocarbons, Oxford University Press, 2002.

Crounse, J. D., Nielsen, L. B., Jørgensen, S., Kjaergaard, H. G., and Wennberg, P. O.: Autoxidation of organic compounds in the atmosphere, The Journal of Physical Chemistry Letters, 4, 3513-3520, 2013.

1014 Dal Maso, M., Kulmala, M., Riipinen, I., Wagner, R., Hussein, T., Aalto, P. P., and Lehtinen, K. E.: Formation
1015 and growth of fresh atmospheric aerosols: eight years of aerosol size distribution data from SMEAR II,
1016 Hyytiala, Finland, Boreal Environment Research, 10, 323, 2005.
1017
1018 Donahue, N. M., Kroll, J., Pandis, S. N., and Robinson, A. L.: A two-dimensional volatility basis set–Part 2:
1019 Diagnostics of organic-aerosol evolution, Atmospheric Chemistry and Physics, 12, 615-634, 2012.
1020
1021 Donahue, N. M., Ortega, I. K., Chuang, W., Riipinen, I., Riccobono, F., Schobesberger, S., Dommen, J.,
1022 Baltensperger, U., Kulmala, M., and Worsnop, D. R.: How do organic vapors contribute to new-particle
1023 formation?, Faraday discussions, 165, 91-104, 2013.
1024
1025 Dusek, U., Frank, G., Hildebrandt, L., Curtius, J., Schneider, J., Walter, S., Chand, D., Drewnick, F., Hings,
1026 S., and Jung, D.: Size matters more than chemistry for cloud-nucleating ability of aerosol particles, Science,
1027 312, 1375-1378, 2006.
1028
1029 Ehn, M., Junninen, H., Petäjä, T., Kurtén, T., Kerminen, V.-M., Schobesberger, S., Manninen, H., Ortega, I.,
1030 Vehkamäki, H., and Kulmala, M.: Composition and temporal behavior of ambient ions in the boreal forest,
1031 Atmospheric Chemistry and Physics, 10, 8513-8530, 2010.
1032
1033 Ehn, M., Junninen, H., Schobesberger, S., Manninen, H. E., Franchin, A., Sipilä, M., Petäjä, T., Kerminen, V.-
1034 M., Tammet, H., and Mirme, A.: An instrumental comparison of mobility and mass measurements of
1035 atmospheric small ions, Aerosol Science and Technology, 45, 522-532, 2011.
1036
1037 Ehn, M., Kleist, E., Junninen, H., Petäjä, T., Lönn, G., Schobesberger, S., Maso, M. D., Trimborn, A., Kulmala,
1038 M., and Worsnop, D.: Gas phase formation of extremely oxidized pinene reaction products in chamber and
1039 ambient air, Atmospheric chemistry and physics, 12, 5113-5127, 2012.
1040

1041 Ehn, M., Thornton, J. A., Kleist, E., Sipilä, M., Junninen, H., Pullinen, I., Springer, M., Rubach, F., Tillmann,
1042 R., and Lee, B.: A large source of low-volatility secondary organic aerosol, Nature, 506, 476, 2014.
1043
1044 Ehn, M., Berndt, T., Wildt, J., and Mentel, T.: Highly Oxygenated Molecules from Atmospheric Autoxidation
1045 of Hydrocarbons: A Prominent Challenge for Chemical Kinetics Studies, International Journal of Chemical
1046 Kinetics, 49, 821-831, 2017.
1047
1048 Frege, C., Ortega, I. K., Rissanen, M. P., Praplan, A. P., Steiner, G., Heinritzi, M., Ahonen, L., Amorim, A.,
1049 Bernhammer, A.-K., and Bianchi, F.: Influence of temperature on the molecular composition of ions and
1050 charged clusters during pure biogenic nucleation, Atmospheric Chemistry and Physics, 18, 65-79, 2018.
1051
1052 Hallquist, M., Wenger, J. C., Baltensperger, U., Rudich, Y., Simpson, D., Claeys, M., Dommen, J., Donahue,
1053 N., George, C., and Goldstein, A.: The formation, properties and impact of secondary organic aerosol: current
1054 and emerging issues, Atmospheric chemistry and physics, 9, 5155-5236, 2009.
1055
1056 Heinritzi, M., Hansel, A., Simon, M., Steiner, G., Wagner, A. C., Kürten, A., and Curtius, J.: submitter:
1057 Characterization of the mass-dependent transmission efficiency of a CIMS, Atmos. Meas. Tech., 9, 1449-
1058 1460, 2016.
1059
1060 Hyttinen, N., Kupiainen-Määttä, O., Rissanen, M. P., Muuronen, M., Ehn, M., and Kurtén, T.: Modeling the
1061 charging of highly oxidized cyclohexene ozonolysis products using nitrate-based chemical ionization, The
1062 Journal of Physical Chemistry A, 119, 6339-6345, 2015.
1063
1064 IPCC: Climate change 2013: the physical science basis. Contribution of the Working Group 1 to the Fifth
1065 Assessment Report (AR5) of the Intergovernmental Panel on Climate Change, edited by: Stocker, T. F., Qin,
1066 D., Plattner, G., Tignor, M., Allen, S., Boschung, J., Nauels, A., Xia, Y., Bex, V., and Midgley, P. M.,
1067 Cambridge University Press, Cambridge (UK), New York (USA), 2013.
1068

1069 Jayne, J. T., Leard, D. C., Zhang, X., Davidovits, P., Smith, K. A., Kolb, C. E., and Worsnop, D. R.:
1070 Development of an aerosol mass spectrometer for size and composition analysis of submicron particles,
1071 Aerosol Science & Technology, 33, 49-70, 2000.
1072
1073 Jenkin, M. E., Saunders, S. M., and Pilling, M. J.: The tropospheric degradation of volatile organic compounds:
1074 a protocol for mechanism development. Atmospheric Environment 31, 81–104, 1997.
1075
1076 Jenkin, M. E., Young, J. C., and Rickard, A. R.: The MCM v3.3.1 degradation scheme for isoprene. Atmos.
1077 Chem. Phys. 15, 11433–11459, 2015.
1078
1079 Jimenez, J. L., Canagaratna, M. R., Donahue, N. M., Prevot, A. S., Zhang, Q., Kroll, J. H., DeCarlo, P. F.,
1080 Allan, J. D., Coe, H., Ng, N. L., Aiken, A. C., Docherty, K. S., Ulbrich, I. M., Grieshop, A. P., Robinson, A.
1081 L., Duplissy, J., Smith, J. D., Wilson, K. R., Lanz, V. A., Hueglin, C., Sun, Y. L., Tian, J., Laaksonen, A.,
1082 Raatikainen, T., Rautiainen, J., Vaattovaara, P., Ehn, M., Kulmala, M., Tomlinson, J. M., Collins, D. R.,
1083 Cubison, M. J., Dunlea, E. J., Huffman, J. A., Onasch, T. B., Alfarra, M. R., Williams, P. I., Bower, K., Kondo,
1084 Y., Schneider, J., Drewnick, F., Borrmann, S., Weimer, S., Demerjian, K., Salcedo, D., Cottrell, L., Griffin,
1085 R., Takami, A., Miyoshi, T., Hatakeyama, S., Shimono, A., Sun, J. Y., Zhang, Y. M., Dzepina, K., Kimmel, J.
1086 R., Sueper, D., Jayne, J. T., Herndon, S. C., Trimborn, A. M., Williams, L. R., Wood, E. C., Middlebrook, A.
1087 M., Kolb, C. E., Baltensperger, U., and Worsnop, D. R.: Evolution of organic aerosols in the atmosphere,
1088 Science, 326, 2009.
1089
1090 Jokinen, T., Sipilä, M., Junninen, H., Ehn, M., Lönn, G., Hakala, J., Petäjä, T., Mauldin Iii, R., Kulmala, M.,
1091 and Worsnop, D.: Atmospheric sulphuric acid and neutral cluster measurements using CI-APi-TOF,
1092 Atmospheric Chemistry and Physics, 12, 4117-4125, 2012.
1093
1094 Jokinen, T., Sipilä, M., Richters, S., Kerminen, V. M., Paasonen, P., Stratmann, F., Worsnop, D., Kulmala,
1095 M., Ehn, M., and Herrmann, H.: Rapid autoxidation forms highly oxidized RO_2 radicals in the atmosphere,
1096 Angewandte Chemie International Edition, 53, 14596-14600, 2014.

1097

1098 Jokinen, T., Berndt, T., Makkonen, R., Kerminen, V.-M., Junninen, H., Paasonen, P., Stratmann, F., Herrmann,
1099 H., Guenther, A. B., and Worsnop, D. R.: Production of extremely low volatile organic compounds from
1100 biogenic emissions: Measured yields and atmospheric implications, Proceedings of the National Academy of
1101 Sciences, 201423977, 2015.

1102

1103 Jordan, A., Haidacher, S., Hanel, G., Hartungen, E., Märk, L., Seehauser, H., Schottkowsky, R., Sulzer, P.,
1104 and Märk, T.: A high resolution and high sensitivity proton-transfer-reaction time-of-flight mass spectrometer
1105 (PTR-TOF-MS), International Journal of Mass Spectrometry, 286, 122-128, 2009.

1106

1107 Julin, J., Winkler, P. M., Donahue, N. M., Wagner P. E., and Riipinen, I.: Near-unity mass accommodation
1108 coefficient of organic molecules of varying structure. Environ. Sci. Technol., 48(20), 12083-12089, 2014.

1109

1110 Junninen, H., Ehn, M., Petäjä, T., Luosujärvi, L., Kotiaho, T., Kostiainen, R., Rohner, U., Gonin, M., Fuhrer,
1111 K., and Kulmala, M.: A high-resolution mass spectrometer to measure atmospheric ion composition,
1112 Atmospheric Measurement Techniques, 3, 1039-1053, 2010.

1113

1114 Kristensen, K., Jensen, L., Glasius, M., and Bilde, M.: The effect of sub-zero temperature on the formation
1115 and composition of secondary organic aerosol from ozonolysis of alpha-pinene, Environmental Science:
1116 Processes & Impacts, 19, 1220-1234, 2017.

1117

1118 Kulmala, M., Kontkanen, J., Junninen, H., Lehtipalo, K., Manninen, H. E., Nieminen, T., Petäjä, T., Sipilä,
1119 M., Schobesberger, S., and Rantala, P.: Direct observations of atmospheric aerosol nucleation, Science, 339,
1120 943-946, 2013.

1121

1122 Kürten, A., Rondo, L., Ehrhart, S., and Curtius, J.: Calibration of a chemical ionization mass spectrometer for
1123 the measurement of gaseous sulfuric acid, The Journal of Physical Chemistry A, 116, 6375-6386, 2012.

1124

Mentel, T. F., Springer, M., Ehn, M., Kleist, E., Pullinen, I., Kurtén, T., Rissanen, M., Wahner, A., and Wildt, J.: Formation of highly oxidized multifunctional compounds: autoxidation of peroxy radicals formed in the ozonolysis of alkenes – deduced from structure–product relationships, Atmos. Chem. Phys., 15, 6745-6765,

Otkjær, R. V., Jakobsen, H. H., Tram, C. M., and Kjaergaard, H. G.: Calculated Hydrogen Shift Rate Constants in Substituted Alkyl Peroxy Radicals, The Journal of Physical Chemistry A, 122, 8665-8673, 2018.

Praske, E., Otkjær, R. V., Crounse, J. D., Hethcox, J. C., Stoltz, B. M., Kjaergaard, H. G., and Wennberg, P. O.: Atmospheric autoxidation is increasingly important in urban and suburban North America, Proceedings of the National Academy of Sciences, 115, 64-69, 2018.

Rissanen, M. P., Kurtén, T., Sipilä, M., Thornton, J. A., Kangasluoma, J., Sarnela, N., Junninen, H., Jørgensen, S., Schallhart, S., and Kajos, M. K.: The formation of highly oxidized multifunctional products in the ozonolysis of cyclohexene, Journal of the American Chemical Society, 136, 15596-15606, 2014.

Rissanen, M. P., Kurtén, T., Sipilä, M., Thornton, J. A., Kausiala, O., Garmash, O., Kjaergaard, H. G., Petäjä, T., Worsnop, D. R., and Ehn, M.: Effects of chemical complexity on the autoxidation mechanisms of endocyclic alkene ozonolysis products: From methylcyclohexenes toward understanding α-pinene, The Journal of Physical Chemistry A, 119, 4633-4650, 2015.

Sarnela, N., Jokinen, T., Duplissy, J., Yan, C., Nieminen, T., Ehn, M., Schobesberger, S., Heinritzi, M., Ehrhart, S., and Lehtipalo, K.: Measurement–model comparison of stabilized Criegee intermediate and highly oxygenated molecule production in the CLOUD chamber, Atmospheric Chemistry and Physics, 18, 2363-2380, 2018.

Saunders, S. M., Jenkin, M. E., Derwent, R. G., and Pilling, M. J.: Protocol for the development of the master chemical mechanism, MCM v3 (part a): tropospheric degradation of non-aromatic volatile organic compounds. Atmos. Chem. Phys., 3**,** 161–180, 2003.

Stolzenburg, D., Fischer, L., Vogel, A. L., Heinritzi, M., Schervish, M., Simon, M., Wagner, A. C., Dada, L., Ahonen, L. R., and Amorim, A.: Rapid growth of organic aerosol nanoparticles over a wide tropospheric temperature range, Proceedings of the National Academy of Sciences, 115, 9122-9127, 2018.

Tang, M. J., Shiraiwa, M., Pöschl, U., Cox, R. A., and Kalberer, M.: Compilation and evaluation of gas phase diffusion coefficients of reactive trace gases in the atmosphere: Volume 2. Diffusivities of organic compounds, pressure-normalised mean free paths, and average Knudsen numbers for gas uptake calculations. Atmos. Chem. Phys., 15, 5585–5598, 2015.

Tröstl, J., Chuang, W. K., Gordon, H., Heinritzi, M., Yan, C., Molteni, U., Ahlm, L., Frege, C., Bianchi, F., and Wagner, R.: The role of low-volatility organic compounds in initial particle growth in the atmosphere, Nature, 533, 527, 2016.

Zhang, Q., Jimenez, J. L., Canagaratna, M., Allan, J., Coe, H., Ulbrich, I., Alfarra, M., Takami, A., Middlebrook, A., and Sun, Y.: Ubiquity and dominance of oxygenated species in organic aerosols in anthropogenically-influenced Northern Hemisphere midlatitudes, Geophysical Research Letters, 34, 2007.

Zhao, J., Ortega, J., Chen, M., McMurry, P., and Smith, J.: Dependence of particle nucleation and growth on high molecular weight gas phase products during ozonolysis of α-pinene, Atmospheric Chemistry and Physics, 13, 9319-9354, 2013.

Appendix

Table A1 : ACCHA Experiment overview

VOC Concentration (ppb)	[VOC] reacted with O3 * (ppb)	[VOC] reacted with OH * (ppb)	Temperature (℃)	Date
		VOC : α- pinene		
50			20	12-Dec-16
50			-15	13-Dec-16
50			0	19-Dec-16
50			-15	21-Dec-16
50	30.1	15.5	20	12-Jan-17
50			-15	13-Jan-17
50	30.0	16.1	0	16-Jan-17
10	6.48	3.04	20	02-Dec-16
10			-15	07-Dec-16
10	6.30	3.14	0	08-Dec-16
10			20 → -15	09-Dec-16
10			-15 → 20	20-Dec-16
		VOC : β-pinene		
50			20	03-Jan-17
50			-15	04-Jan-17
50			0	05-Jan-17

* Estimation based on model simulations using the Master Chemical Mechanism v3.3.2 (Jenkin et al.,1997 & 2015; Saunders et al., 2003)

Table A2: Main monoterpene ozonolysis HOM products: Peak list

Monomers		Dimers					
m/z (Th)	Composition*	**m/z** (Th)	Composition*	**m/z** (Th)	Composition*	**m/z** (Th)	Composition*
308.06	$C_{10}H_{14}O_7$	**446.17**	$C_{19}H_{28}O_8$	**514.14**	$C_{18}H_{28}O_{13}$	**562.13**	$C_{18}H_{28}O_{16}$
309.07	$C_{10}H_{15}O_7$	**448.18**	$C_{19}H_{30}O_8$	**514.18**	$C_{19}H_{32}O_{12}$	**572.15**	$C_{20}H_{30}O_{15}$
310.08	$C_{10}H_{16}O_7$	**462.16**	$C_{19}H_{28}O_9$	**516.16**	$C_{18}H_{30}O_{13}$	**574.13**	$C_{19}H_{28}O_{16}$
324.06	$C_{10}H_{14}O_8$	**464.18**	$C_{19}H_{30}O_9$	**524.13**	$C_{18}H_{26}O_{13}$	**574.16**	$C_{20}H_{32}O_{15}$
325.07	$C_{10}H_{15}O_8$	**466.16**	$C_{18}H_{28}O_{10}$	**524.16**	$C_{20}H_{30}O_{12}$	**576.14**	$C_{19}H_{30}O_{16}$
326.07	$C_{10}H_{16}O_8$	**478.16**	$C_{19}H_{28}O_{10}$	**526.14**	$C_{19}H_{28}O_{13}$	**578.12**	$C_{18}H_{28}O_{17}$
340.05	$C_{10}H_{14}O_9$	**480.17**	$C_{19}H_{30}O_{10}$	**526.18**	$C_{20}H_{32}O_{12}$	**588.11**	$C_{19}H_{26}O_{17}$
341.06	$C_{10}H_{15}O_9$	**482.15**	$C_{18}H_{28}O_{11}$	**528.16**	$C_{19}H_{30}O_{13}$	**588.14**	$C_{20}H_{30}O_{16}$
342.07	$C_{10}H_{16}O_9$	**486.15**	$C_{17}H_{28}O_{12}$	**530.14**	$C_{18}H_{28}O_{14}$	**590.16**	$C_{20}H_{32}O_{16}$
356.05	$C_{10}H_{14}O_{10}$	**492.17**	$C_{20}H_{30}O_{10}$	**540.12**	$C_{19}H_{26}O_{14}$	**592.14**	$C_{19}H_{30}O_{17}$
357.05	$C_{10}H_{15}O_{10}$	**494.15**	$C_{19}H_{28}O_{11}$	**540.16**	$C_{20}H_{30}O_{13}$	**594.12**	$C_{18}H_{28}O_{18}$
358.06	$C_{10}H_{16}O_{10}$	**494.19**	$C_{20}H_{32}O_{10}$	**542.14**	$C_{19}H_{28}O_{14}$	**604.14**	$C_{20}H_{30}O_{17}$
372.04	$C_{10}H_{14}O_{11}$	**496.17**	$C_{19}H_{30}O_{11}$	**542.17**	$C_{20}H_{32}O_{13}$	**606.12**	$C_{19}H_{28}O_{18}$
373.05	$C_{10}H_{15}O_{11}$	**498.15**	$C_{18}H_{28}O_{12}$	**544.15**	$C_{19}H_{30}O_{14}$	**606.15**	$C_{20}H_{32}O_{17}$
374.06	$C_{10}H_{16}O_{11}$	**498.18**	$C_{19}H_{32}O_{11}$	**546.13**	$C_{18}H_{28}O_{15}$	**608.13**	$C_{19}H_{30}O_{18}$
		502.14	$C_{17}H_{28}O_{13}$	**546.17**	$C_{19}H_{32}O_{14}$	**620.10**	$C_{19}H_{26}O_{19}$
		508.17	$C_{20}H_{30}O_{11}$	**556.15**	$C_{20}H_{30}O_{14}$	**620.13**	$C_{20}H_{30}O_{18}$
		510.15	$C_{19}H_{28}O_{12}$	**558.13**	$C_{19}H_{28}O_{15}$	**622.15**	$C_{20}H_{32}O_{18}$
		510.18	$C_{20}H_{32}O_{11}$	**558.17**	$C_{20}H_{32}O_{14}$		
		512.16	$C_{19}H_{30}O_{12}$	**560.15**	$C_{19}H_{30}O_{15}$		

* Note that all compounds are detected as cluster with Nitrate Ion (NO_3^-)